The Seismicity of Indonesia

Sean J. Hutchings[1], Walter D. Mooney[1]

[1]United States Geological Survey, Earthquake Science Center, Menlo Park, CA

Corresponding Author: Sean Hutchings (sean@hutchnsuch.net)

Key Points:

- We summarize the current knowledge of Indonesian seismotectonics by documenting distributions of hypocenters and focal mechanisms.
- Intermediate and deep seismicity traces Wadati-Benioff zones of subducting slabs with geometry consistent with recent tomography models.
- Shallow seismicity generated by diverse faulting is consistent with regional tectonic and faulting models, posing seismic hazards.

Abstract

Indonesian seismicity provides important insights into the tectonics and hazards of a region that is characterized by a remarkable diversity in faulting, including subduction, extension, thrusting, and strike-slip faulting. We present a synthesis of Indonesian seismotectonics by documenting the distributions of hypocenters (≥ **M** 4.6) and focal mechanisms (≥ **M** 5.0) over ~20 years, quantifying seismicity rates, and comparing observed seismicity trends with proposed tectonic models. Of the 20,622 events ≥ **M** 4.6 observed in the study region, ~77% of seismicity are shallow (≤ 70 km depth) and of magnitudes < **M** 5.0 (68%). 61 events ≥ **M** 7.0 occurred, four of which exceeded **M** 8.0, including the 2004 $\mathbf{M}_w$ 9.1 Sumatra-Andaman earthquake. Regionally, about ~320 ≥ **M** 5.0 earthquakes occur per year, and rates decrease exponentially between 50-300 km with significantly elevated seismicity in the Mantle Transition Zone (MTZ). Intermediate and deep events (≥ 70 km depth) trace the Wadati-Benioff zones of several subducting slabs exhibiting a geometry consistent with recent tomography models. Seismicity extends to a maximum depth of 678 km. Oblique convergence, lithospheric age, ambient mantle temperatures and viscous resistance at the 410, 520, and 660 km phase boundaries likely contribute to the non-uniform depth distribution of intermediate and deep earthquakes. Shallow seismicity provides insight into how complex oblique convergence is accommodated near the surface, with primary sources including megathrusting, crustal faulting, and shallow intraslab faulting. All sources of shallow seismicity constitute significant seismic hazards.

Plain Language Summary

Indonesia and much of southeastern Asia experiences frequent earthquakes produced by a variety of sources and is highly prone to earthquake hazards. We summarize the geographic distribution, sources, and frequency of earthquakes throughout the Indonesian region over a 20-year period, document associated hazards, and highlight the relevance to regional plate tectonic models. Indonesia and neighboring areas experience an annual average of about 320 earthquakes with magnitudes ≥ 5.0, and three events of magnitudes ≥ 7.0. The majority of all earthquakes occur at depths ≤ 70 km, although deeper earthquakes ≥ 70 km are common, extending to ~678 km at the deepest. Several of the largest instrumentally recorded earthquakes occurred in Indonesia, including four events with magnitudes ≥ 8.0 since January 2000, the most destructive

being the 2004 $\mathbf{M}_w$ 9.1 Sumatran-Andaman earthquake. The frequency of strong earthquakes at depths ≤ 70 km poses a serious risk from ground shaking, tsunamis and landslides for Indonesian communities.

Keywords: Megathrust earthquakes, intermediate and deep earthquakes, Sumatra, Java, Banda Sea, Celebes Sea

1 Introduction

The seismicity of Indonesia and the surrounding area provides crucial evidence for the active tectonic processes of this region. Indonesia lies at the intersection of the obliquely converging Indo-Australian, Philippine Sea, Caroline, and Sunda plates (Figure 1). In western Indonesia the Indo-Australian plate subducts northward beneath the Sunda plate at the Sunda-Java trench. In eastern Indonesia, plate convergence is partitioned among several microplates forming a zone of deformation characterized by subduction, strike-slip, thrust, and extensional faulting (Figure 1; Rangin et al., 1999; Charlton, 2000; Bird, 2003; Bock et al., 2003; Hinschberger et al., 2005; Hall, 2012; Watkinson and Hall, 2017; Hall, 2018). The region exhibits a high rate of seismicity, experiencing on average ~18 major magnitude events (≥ **M** 7.0) per decade, with 15 great magnitude events (≥ **M** 8.0) occurring since 1900 (U.S. Geological Survey, 2020).

Elevated seismic activity, particularly in the past two decades, has produced four great magnitude events, the largest being the December 26, 2004 $\mathbf{M}_w$ 9.1 Great Sumatra-Andaman earthquake and tsunami (Lay et al., 2005), and several other damaging events motivating a need to further understand Indonesian seismicity and associated hazards. Numerous recent studies have been conducted to better understand Indonesian seismicity and tectonics, identifying and imaging sources of seismicity such as subduction zones and crustal faults (Charlton, 2000; Sieh and Natawidjaja, 2000; Bock et al., 2003; Hinschberger et al., 2005; Soquet et al., 2006; Spakman and Hall, 2010; Watkinson et al., 2011; Widiyantoro et al., 2011a,b; Hall, 2012; Hall and Spakman, 2015; Omang et al., 2016; Koulali et al., 2016; Cipta et al., 2016; Bradley et al., 2017; Watkinson and Hall, 2017; Fan and Zhao, 2018; Supendi et al., 2018; Hall, 2018; Patria and Putra, 2020; Irsyam et al., 2020). However, no recent study provides a comprehensive summary of seismicity for all of Indonesia. To fill this gap, we investigate the distributions of hypocenters and focal mechanisms spatially and with depth, quantify seismicity rates, and

compare observed trends to proposed tectonic models to synthesize a comprehensive summary of Indonesian seismotectonics.

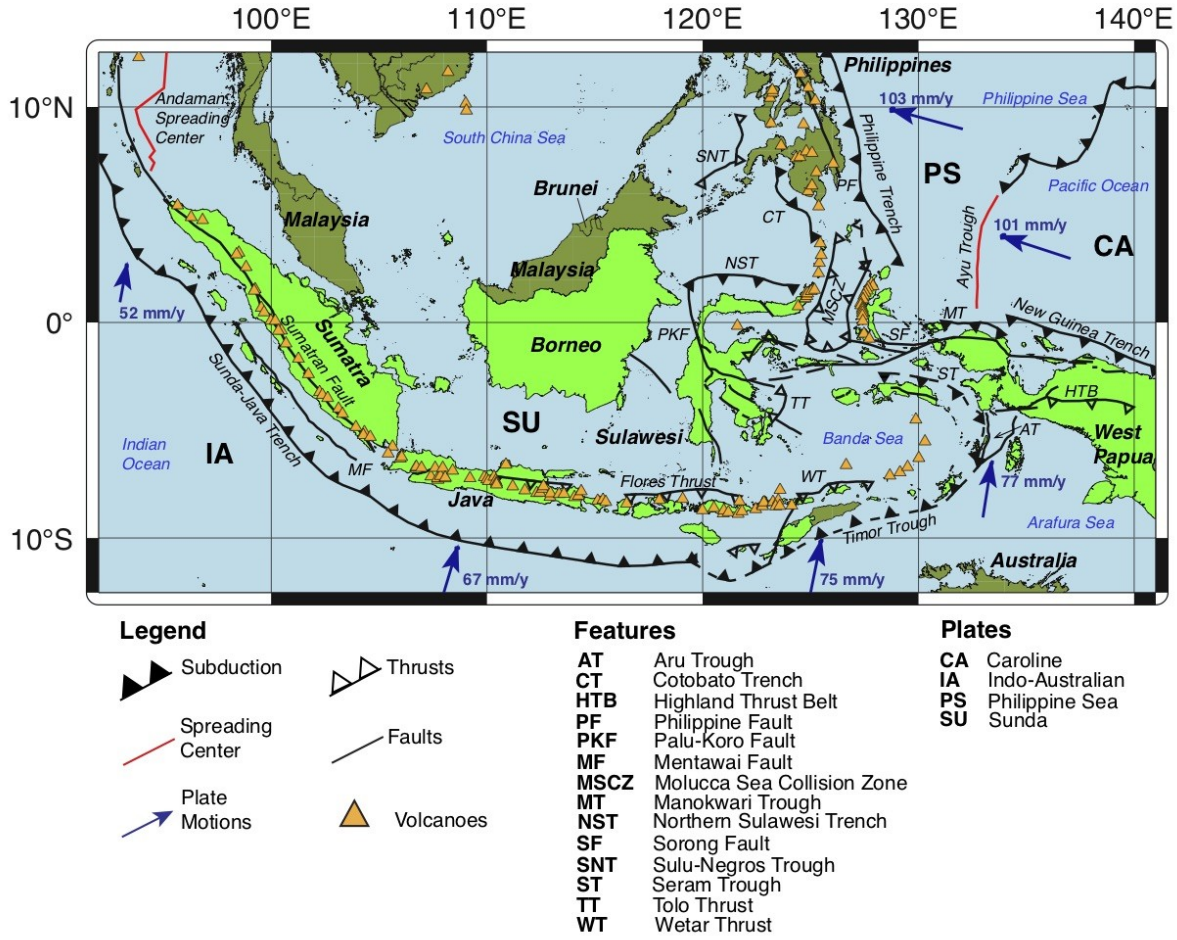

Figure 1. Tectonic setting of Indonesia and the surrounding region. Indonesia is highlighted in green. Locations of plates, boundaries and faults are shown. Indonesia lies at the point of convergence between the Indo-Australian, Sunda, Philippine Sea, and Caroline plates. Subduction is prevalent. Plate velocities are with respect to the Sunda plate obtained from the MORVEL velocity model (DeMets et al., 2010). Faults and boundaries are obtained from Moore and Silver (1983), Silver et al. (1983a,b), Widiwijayanti et al. (2004), Besana and Ando (2005), Roosmawati and Harris (2009), Watkinson et al. (2011), Hall (2012), Mukti et al. (2012), Tsutsumi and Perez (2013), Saputra et al. (2014), Cipta et al. (2016), Koulali et al. (2016), Omang et al. (2016), Adhitama et al. (2017), Patria and Hall (2017), Watkinson and Hall (2017), Hall (2018), Nugraha and Hall (2018), Supendi et al. (2018), and Valkaniotis et al. (2018).

2 Tectonic Setting

The study area is located between 92˚-141˚E and 12.5˚S-12.5˚N (Figure 1). The tectonics of Indonesia is commonly divided into western and eastern settings. Plate motions, tectonic boundaries and major faults are displayed in Figure 1. Relative to the Sunda plate, the Indo-Australian plate moves NNE at ~52 – 77 mm/y, and the Philippine Sea plate ~101 – 103 mm/y WNW (Figure 1; DeMets et al., 2010). The Caroline plate exhibits motion similar to the Philippine Sea plate, with minor relative motion between them due to spreading at the Ayu trough (Figure 1; Bird, 2003; DeMets et al., 2010). West of ~120˚E, the Indo-Australian plate subducts beneath the Sunda plate at the Sunda-Java trench with convergence nearly orthogonal south of Java (~110˚E) and oblique farther west (Bock et al., 2003; McCaffrey, 2009). East of 120˚E, subduction transitions to collision between the Indo-Australian and Sunda plates at the Timor and Seram troughs (ST; Figure 1; Audley-Charles, 2011). The Philippine Sea plate subducts beneath the Sunda plate at the Philippine trench, and the Caroline plate subducts beneath West Papua at the New Guinea trench (Figure 1). Subduction is also active within the Northern Sulawesi trench (NST) and Cotobato trench (CT; Hall, 2018). In addition to subduction, crustal fault zones such as the Sorong (SF) and Palu-Koro faults (PKF) in eastern Indonesia and the Sumatran fault in western Indonesia accommodate convergence within the overriding plates (Bradley et al., 2017; Watkinson and Hall, 2017).

3 Data and Methods

Hypocenter locations for all events ≥ **M** 4.0 that occurred in this region between January 1, 2000 and July 28, 2020 (~20.6 years) are obtained from the U.S. Geological Survey (USGS) Advanced National Seismic System (ANSS) Comprehensive Catalog (ComCat; U.S. Geological Survey, 2020). Using the b-value stability method (Cao and Gao, 2002; Mignan and Woessner, 2012), we estimate a magnitude of completeness (M_c) for the ANSS catalog in this region of **M** 4.6, and thus only events ≥ **M** 4.6 are used in our analysis. Focal mechanism solutions are obtained for the same time period for events ≥ **M** 5.0 (approximate magnitude of completeness) from the Global Centroid Moment Tensor (GCMT) Project Catalog (Dziewonski et al., 1981; Ekström et al., 2012). When referring to USGS hypocenter magnitudes, **M** constitutes a mix of moment ($\mathbf{M}_w$) and body wave ($\mathbf{M}_b$) magnitudes, where $\mathbf{M}_w$ comprises ~60% of events ≥ **M** 5.0 and $\mathbf{M}_b$ comprises ~96% of events < **M** 5.0. When referring to GCMT magnitudes, **M** is moment magnitude $\mathbf{M}_w$ (Ekström et al., 2012). Locations of major Holocene volcanic centers are obtained

from the Smithsonian Global Volcanism Program Catalog (Global Volcanism Program, 2013). All maps are generated using Generic Mapping Tools (GMT) open-source software version 6.0 (Wessel et al., 2019). Topography and bathymetry data are plotted as 30 arc second resolution global relief grids (derived from Tozer et al., 2019) accessed as remote data sets through GMT (Wessel et al., 2019).

Seismicity is analyzed by plotting hypocenters and focal mechanisms in reference to published fault traces and tectonic boundaries, in cross-section, and by quantifying average seismicity rates in earthquakes/year (EQ/y). Seismicity rates are computed for all events ≥ **M** 5.0 and plotted against depth (km) in histograms with 10-km depth bins normalized by the 20.6-year data window. Curve fits are of the form $log_{10}(y) = a - bx$. Seismicity rates for individual subregions are determined from hypocenters within approximately equal-area sectors (~$1x10^6$ km^2). Gutenberg-Richter distributions are obtained using the equation $log_{10}(N) = a - b(M-M_c)$, where N is the sum of events of a given magnitude, a and b are constants, M is magnitude and M_c is the magnitude of completeness.

Owing to the abundance of the seismicity, it is divided into (1) intermediate and deep seismicity (≥ 70 km depth), and (2) shallow seismicity (≤ 70 km depth). Intermediate and deep hypocenters are plotted in cross-section and compared to Slab 2.0 geometries (Hayes, 2018) and tomography models (Spakman and Hall, 2010; Widiyantoro et al., 2011a,b; Hall and Spakman, 2015; Fan and Zhao, 2018). Cross-sections are constructed from projected hypocenters located 50 km on either side of the section lines with 1:1 scaling. Shallow seismicity is analyzed using focal mechanisms to compare observed faulting with tectonic and faulting models (Moore and Silver, 1983; Silver et al., 1983a,b; Rangin et al., 1999; Charlton, 2000; Sieh and Natawidjaja, 2000; Charlton, 2000; Bird, 2003; Bock et al., 2003; Hinschberger et al., 2005; Soquet et al., 2006; Watkinson et al., 2011; Hall, 2012; Saputra et al., 2014; Cipta et al., 2016; Watkinson and Hall, 2017; Patria and Hall, 2017; Bradley et al., 2017; Hall, 2018; Valkaniotis et al., 2018).

3.1 Sources of Uncertainty

The following sources of uncertainty in our analysis have been identified.

(1) USGS hypocenters. Our completeness estimate of the USGS catalog in Indonesia provides confidence that hypocenters as low as **M** 4.6 are well located, though it is important to note discrepancies between earthquake catalogs. As hypocenter locations are a key component of

this study, we estimate location uncertainty by comparing a subset of 450 USGS locations of varying magnitudes ≥ **M** 4.6 and depths with equivalent locations in the International Seismological Centre (ISC) Bulletin (International Seismological Centre, 2021). From this comparison, latitude and longitude variances between the catalogs are generally small, varying on average between +- 0.09˚ - 0.14˚ (~5-13 km) and +- 0.05˚ - 0.07˚ (~5-8 km) respectively. Hypocentral depths for shallow, intermediate and deep events vary on average by +- 12 km, +- 16 km, and +- 9 km respectively. Deep events exhibit the lowest depth variances. Conversely, intermediate events exhibit the largest depth variances (~ 22% of tested events exhibit depth differences > 20 km, with a maximum variance of 165 km). These variances reflect event relocations conducted by ISC (Storchak et al., 2020). Therefore, some events in the USGS catalog may have poorly resolved depths, such as those with default depths of 10 km and 33 km assigned. This may introduce some bias to our analysis, primarily to seismicity rate calculations and cross-sections.

(2) Cross-sections. In addition to hypocenter location uncertainty, the chosen 100 km – wide swath of hypocenters projected on section lines may introduce some minor bias to the cross-sections, especially if there is enough curvature or along-strike changes in slab orientation within the 100 km area. Efforts were made to draw cross-sections orthogonal to the subduction zone strike.

(3) GCMT focal mechanisms. GCMT source mechanism solutions have been shown recently to be consistent and robust for events ≥ **M** 5.0, with significant improvements added to the CMT method since 2004 that include increased station coverage, consideration of intermediate-period surface waves and addressing heterogeneity in earth models (Ekström et al., 2012; Ekström, 2015). Though the majority of events used in our analysis occurred during or after implementation of these improvements (post 2004), we do use prior events (2000-2004) that may therefore be less accurate (Ekström et al., 2012). In addition, fewer events are available between 2000 and 2004, as the completeness of the GCMT catalog prior to 2004 is estimated at ~**M** 5.3-5.4 (Ekström et al., 2012). Despite this, we are confident in the accuracy of GCMT source mechanisms for use in our analysis. Additionally, there will be location discrepancies noticed between USGS hypocenters and GCMT solutions. GCMT solutions plot the location of the centroid, or location of max stress release during an earthquake (Dziewonski et al., 1981; Ekström et al., 2012), and often do not correspond exactly with the location of the hypocenter

(point of earthquake initiation). In comparing the locations of 300 equivalent events ≥ **M** 5.0 between the USGS and GCMT catalogs, we find that latitude and longitude vary on average by +- 0.08-0.16 ˚ (9-18 km) and +- 0.1-0.13˚ (11-14 km) respectively, and depth locations for shallow, intermediate and deep events vary on average by +- 9 km, +- 12 km, and +- 9 km respectively. These variances may make it difficult to associate some events with particular faults.

(4) Fault and plate boundary locations. The locations of some faults and plate boundaries in Indonesia are greatly debated, and so differing interpretations are common. The faults and plate boundaries plotted on the maps used in this study are obtained from several published studies, and these provide the tectonic context of the seismicity. Here we assume the most up-to-date published placement of the faults are correct and we do not attempt to re-assign fault locations.

4 Seismicity

4.1 General Trends

Indonesia's dense seismic activity is primarily concentrated at or near the plate boundaries, with events increasing in depth inboard of major subduction zones (Figures 1 and 2a). Figure 2a shows the locations of the 20,622 events ≥ **M** 4.6 that occurred in the region over the 20.6-year time period. Hypocenter depths range from ≤ 10 km to 678 km. The majority of events occur at depths ≤ 70 km (Table 1), and are of magnitudes < **M** 5.0 (Table 2), comprising 77% and 68% of the total events respectively. Events ≥ **M** 7.0 are not uncommon (Figure 2b), with 61 events occurring since January 2000, the largest being the 2004 $\mathbf{M}_w$ 9.1 Great Sumatra-Andaman Earthquake (Tables 2 and 3; Lay et al., 2005; Hayes et al., 2017; U. S. Geological Survey, 2020). Table 3 lists notable events ≥ **M** 7.0 shown in Figure 2b. The Gutenburg-Richter distribution of the data (Figure 3a) exhibits a b-value of 1.2, implying a greater frequency of low-magnitude events than expected (perfect distribution exhibits a b-value of 1).

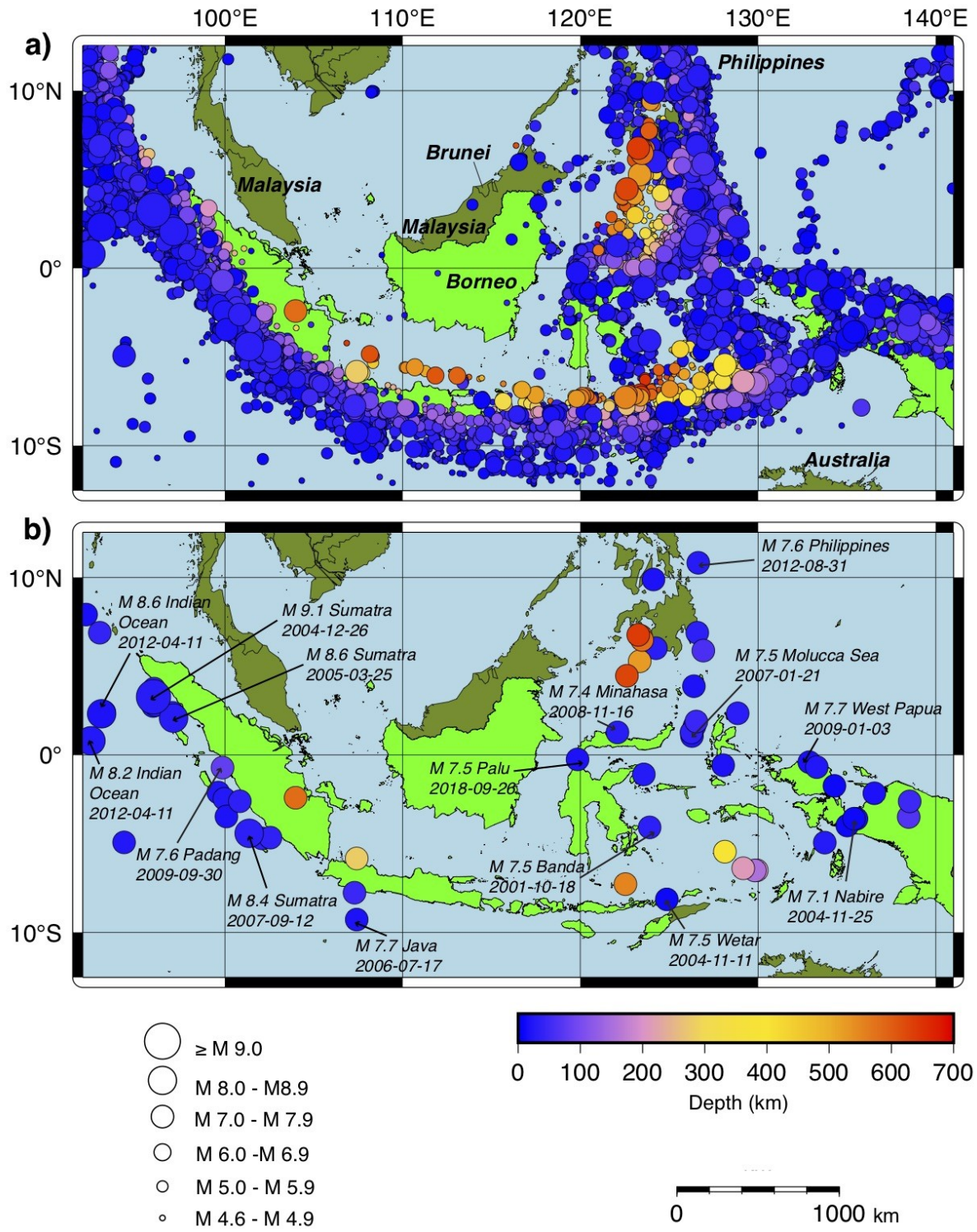

Figure 2. Seismicity of Indonesia and neighboring regions for all events (a) ≥ **M** 4.6, and (b) ≥ **M** 7.0 between January 1, 2000 and July 28, 2020 (U.S. Geological Survey, 2020). The majority of events are shallow, of relatively low magnitude (< **M** 6.0), and concentrated near the plate

boundaries. Events ≥ **M** 7.0 are not uncommon. Hypocenters are colored by depth and are scaled by magnitude. More information for notable events labeled in panel (b) is presented in Table 3.

Table 1

Number of Earthquakes by Depth (km)

Depth Range	Number of Events	Percentage of Total
All	20622	100%
Shallow (0-70 km)	15970	77.4%
Intermediate (70-300 km)	4073	19.8%
Deep (> 300 km)	579	2.8%

Table 2

Number of Earthquakes by Magnitude

Magnitude Range	Number of Events	Percentage of Total
4.6 – 4.9	14068	68.218%
5.0 – 5.4	4857	23.553%
5.5 – 5.9	1187	5.756%
6.0 – 6.4	350	1.697%
6.5 – 6.9	99	0.480%
7.0 – 7.4	35	0.170%
7.5 – 7.9	21	0.102%
8.0 – 8.4	2	0.001%
8.5 – 8.9	2	0.001%
9.0 – 9.4	1	0.005%

Table 3

List of Earthquakes ≥ M_w 7.0 between January 1, 2000 and July 28, 2020

Date	Location	Latitude	Longitude	Depth (km)	Magnitude (M_w)	Mechanism
December 26, 2004	Aceh, Sumatra	3.295	95.982	30	9.1 (Duputel et al., 2012)	Thrust †*^
March 28, 2005	Nias, Sumatra	2.085	97.108	30	8.6	Thrust †*
April 11, 2012	Indian Ocean (NW Sumatra)	2.327	93.063	20	8.6 (Duputel et al., 2012)	Strike-slip †* (Satriano et al., 2012)
September 12, 2007	Bengkulu, Sumatra	-4.438	101.367	34	8.4 (Duputel et al., 2012)	Thrust †*
April 11, 2012	Indian Ocean (NW Sumatra)	0.802	92.463	25.1	8.2	Strike-slip*
September 12, 2007	Mentawai, Sumatra	-2.625	100.841	35	7.9	Thrust †
June 4, 2000	Enganno, Sumatra	-4.721	102.087	33	7.9	Strike-slip-reverse †^ (Abercrombie et al., 2003)
March 2, 2016	Indian Ocean (SW of Sumatra)	-4.952	94.33	24	7.8	Strike-slip
October 25, 2010	Kepulauan Mentawai	-3.487	100.082	20.1	7.8	Thrust †*
April 6,	Aceh, Sumatra	2.383	97.048	31	7.8	Thrust*

2010						
January 3, 2009	Manokwari, West Papua	-0.414	132.885	17	7.7	Thrust †*
July 17, 2006	Java	-9.284	107.419	20	7.7	Thrust †*
July 23, 2010	Mindanao, Philippines	6.497	123.480	578	7.6	Oblique normal
January 27, 2006	Banda Sea	-5.473	128.131	397	7.6	Oblique normal
September 30, 2009	Padang, Sumatra	-0.72	99.867	81	7.6	Oblique reverse †^ (Wiseman et al., 2012)
October 10, 2002	Manokwari, West Papua	-1.757	134.297	10	7.6	Strike-slip †*^
August 31, 2012	Mindanao (Philippines)	10.811	126.638	28	7.6	Thrust †*^ (Ye et al., 2012)
May 4, 2000	Banggai Islands (Sulawesi)	-1.105	123.573	26	7.6	Strike-slip †*
September 28, 2018	Palu, Sulawesi	-0.256	119.846	20	7.5	Strike-slip †*^
August 8, 2007	Jakarta, Java	-5.859	107.419	280	7.5	Oblique reverse
January 21, 2007	Molucca Sea	1.065	126.282	22	7.5	Reverse †
July 23, 2010	Moro Gulf, Mindanao	6.776	123.259	640.6	7.5	Oblique normal
October 19, 2001	Banda Sea	-4.102	123.907	33	7.5	Strike-slip
November 11, 2004	Wetar Area	-8.152	124.868	10	7.5	Thrust †^
March 5, 2002	West Mindanao, Philippines	6.033	124.249	31	7.5	Oblique reverse †*
January 1, 2001	East Mindanao, Philippines	6.898	126.579	33	7.5	Oblique reverse
November 16, 2008	Minahasa, Sulawesi	1.271	122.091	30	7.4	Thrust †
January 3, 2009	Manokwari, West Papua	-0.691	133.305	23	7.4	Thrust †
February 20, 2008	Simeulue, Sumatra	2.768	95.964	26	7.4	Thrust †
November 2, 2002	Simeulue, Sumatra	2.824	96.085	30	7.4	Thrust †
February 13, 2001	Bengkulu, Sumatra	-4.680	102.562	36	7.4	Thrust
June 24, 2019	Banda Sea	-6.408	129.169	212	7.3	Strike-slip
January 10, 2017	Celebes Sea	4.478	122.617	627.2	7.3	Oblique reverse
July 23, 2010	West Mindanao, Philippines	6.718	123.409	607.1	7.3	Oblique normal
July 25, 2004	Palembang, Sumatra	-2.427	103.981	582.1	7.3	Oblique normal
February 7, 2004	Nabire, West Papua	-4.003	135.023	10	7.3	Strike-slip †
July 14,	South Halmahera	-0.586	128.034	19	7.2	Strike-slip †*^

2019	Island					
January 10, 2012	Indian Ocean near Aceh, Sumatra	2.433	93.210	19	7.2	Strike-slip
May 9, 2010	Aceh, Sumatra	3.748	96.018	38	7.2	Thrust †
February 11, 2009	Talaud Island	3.886	126.387	20	7.2	Reverse †
February 25, 2008	Mentawai, Sumatra	-2.486	99.972	25	7.2	Thrust
December 26, 2004	Nicobar Islands	6.910	92.958	39.2	7.2	Oblique reverse
November 14, 2019	Molucca Sea	1.621	126.416	33	7.1	Reverse †*
February 5, 2005	Celebes Sea	5.293	123.337	525	7.1	Normal
December 10, 2012	Banda Sea	-6.533	129.825	155	7.1	Strike-slip
March 2, 2005	Banda Sea	-6.527	129.933	201.7	7.1	Oblique
November 26, 2004	Nabire, West Papua	-3.609	135.404	10	7.1	Oblique †
February 24, 2001	Molucca Sea	1.271	126.249	35	7.1	Reverse
October 15, 2013	Sagabayan, Philippines	9.880	124.117	19	7.1	Oblique reverse †
November 15, 2014	Mayu, Molucca Sea	1.893	126.522	45	7.1	Reverse
December 29, 2018	East Mindanao, Philippines	5.898	126.921	60.2	7.0	Oblique reverse
July 27, 2015	Abepura, West Papua	-2.629	138.528	48	7.0	Reverse †
February 27, 2015	Flores	7.297	122.535	552.1	7.0	Strike-slip
June 16, 2010	Yapen, West Papua	-2.174	136.543	18	7.0	Strike-slip †^
September 29, 2010	Aru Trough	-4.963	133.760	26	7.0	Normal
September 13, 2007	Mentawai, Sumatra	-2.130	99.627	22	7.0	Thrust †
September 2, 2009	Java	-7.782	107.297	46	7.0	Oblique reverse †*^
February 5, 2004	Nabire, West Papua	-3.615	135.538	16.6	7.0	Oblique normal †
May 26, 2003	Morotai, Halmahera	2.354	128.855	31	7.0	Reverse †
April 6, 2013	Enarotali, West Papua	-3.517	138.476	66	7.0	Oblique normal
August 5, 2018	Lombok	-8.258	116.438	34	6.9	Thrust †*
August 19, 2018	Lombok	-8.319	116.627	21	6.9	Thrust †
December 6, 2016	Aceh, Sumatra	5.283	96.168	13	6.6 (Salman et al., 2020)	Strike-slip † (Salman et al., 2020)
October 1,	Bengkulu, Sumatra	-2.482	101.524	9.0	6.6	Strike-slip † (Salman et

2009						al., 2020)
September 25, 2019	Ambon, Seram	-3.453	128.370	12.3	6.5	Strike-slip †^

Note. Events are presented in order of magnitude ($\mathbf{M}_w$). "†" indicates damage was caused. "*" indicates tsunami generation. "^" indicates landslide/liquefaction generation. A few notable events ≤ $\mathbf{M}_w$ 7.0 are included. Event location, depth, magnitude, and mechanism are obtained from the USGS ANSS ComCat Catalog, unless otherwise indicated (Hayes et al., 2017; U.S. Geological Survey, 2020).

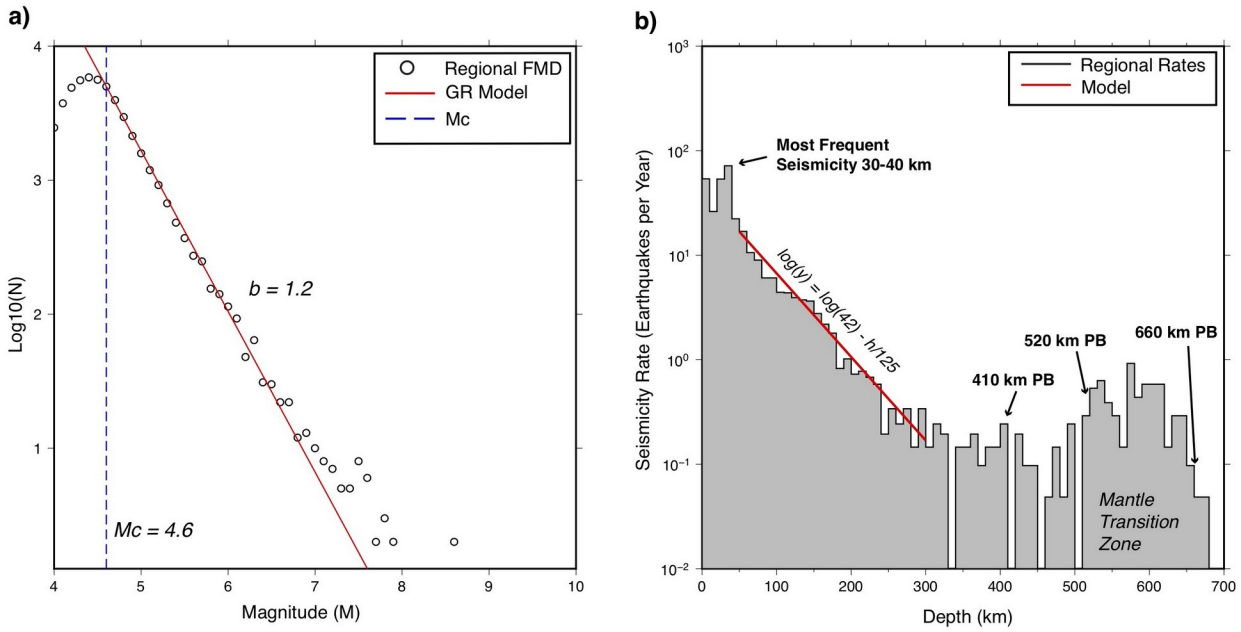

Figure 3. (a) Gutenberg-Richter distribution for events ≥ **M** 4.0. The estimated magnitude of completeness (M_c) is 4.6, obtained by the b-value stability method (Cao and Gao, 2002; Mignan and Woessner, 2012). The frequency-magnitude distribution (FMD) for events ≥ **M** 4.6 (Figure 2a) is modeled by the Gutenberg-Richter equation $log_{10}(N) = 1.6 – 1.2(M – 4.6)$, where N is the sum of events of magnitude M. The b-value is 1.2, implying a greater frequency of lower magnitude events than expected. (b) Histogram of regional seismicity rates distributed with depth for all events ≥ **M** 5.0 between January 2000 and July 2020 (Table 4). Events are most frequent between 30-40 km depth, with frequency decreasing exponentially between 50-300 km. Seismicity increases again within the Mantle Transition Zone (MTZ). Depth bins (x-axis) are 10 km wide, and the y-axis is log-scaled. Locations of the 410, 520, and 660 km phase boundaries in the MTZ are indicated.

4.2 Seismicity Rates

Seismic activity varies greatly with location and depth. For example, earthquakes approaching the lower mantle (~660 km) are abundant in eastern Indonesia, but are not present in western Indonesia (Figure 2a). These trends in seismic activity can be more closely observed by quantifying seismicity rates with depth. Seismicity rates provide insight into the most seismically active regions and how activity changes with depth, and are compared between the entire study region (Figure 3b) and seven individual subregions (Figure 4). Subregions are divided into west and east Indonesian subregions (Figures 4b-c). All calculated seismicity rates are presented in Table 4.

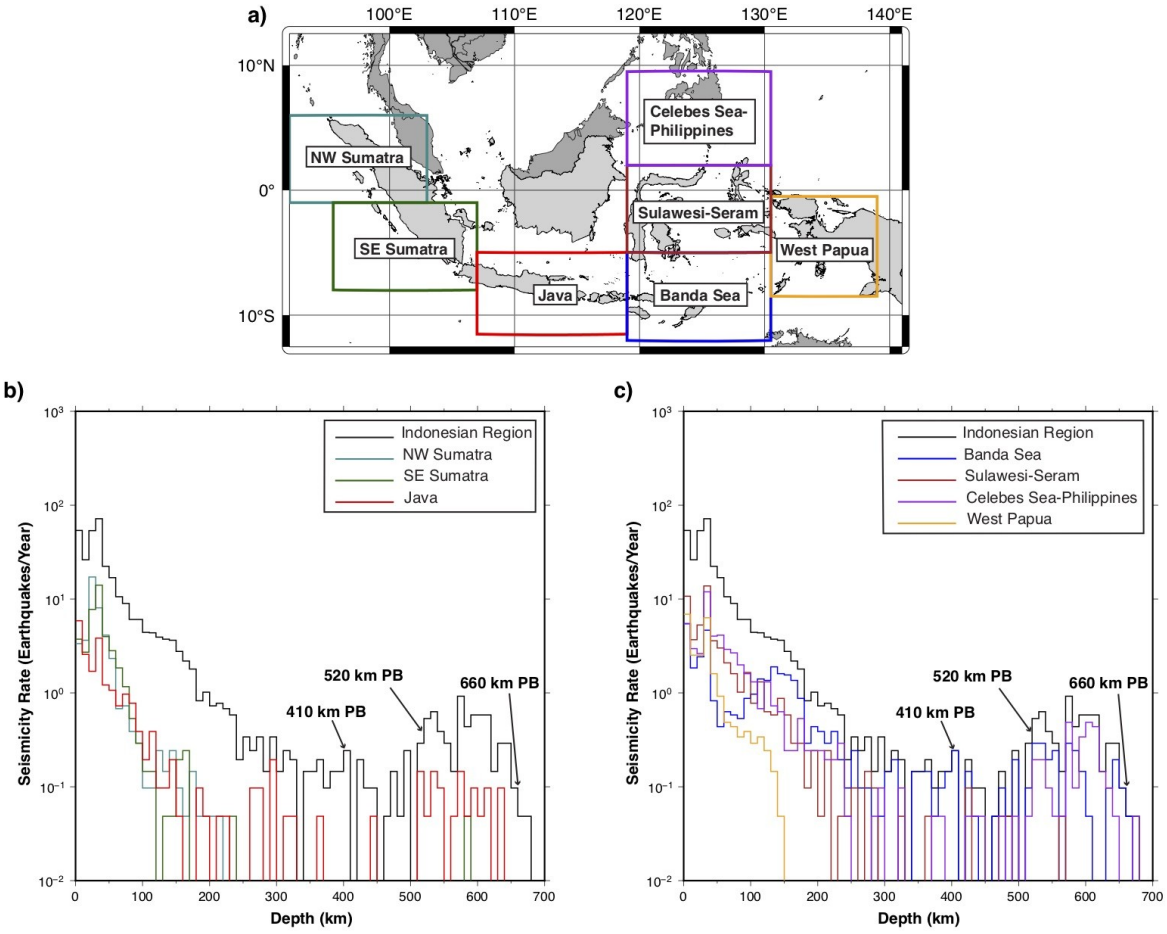

Figure 4. Indonesian subregion seismicity rates for all events ≥ **M** 5.0 between January 1, 2000 and July 28, 2020. (a) Subregion boundaries. Each subregion is approximately 1x10^6 km^2 in area and colored to match respective histograms. (b) Seismicity rates with depth for western Indonesian subregions. NW Sumatra exhibits the highest seismicity rate between 20-30 km.

Intermediate and deep seismicity (≥ 70 km) increases eastward toward Java. (c) Seismicity rates for eastern Indonesian subregions. The majority of MTZ seismicity is located in the Banda Sea and Celebes Sea-Philippines. For both (b) and (c), the regional average distribution (Figure 3b) is shown and the 410, 520, and 660 km phase boundaries (PB) are labeled. Depth bins are 10 km wide and the y-axis is log-scaled. Rate values are presented in Table 4.

Table 4

Calculated Seismicity Rates

Region	Regional Average	NW Sumatra	SE Sumatra	Java	Banda Sea	Molucca Sea	Celebes Sea	West Papua
Depth Range (km)								
0-10	53.786	3.350	3.738	5.874	5.485	10.728	5.437	6.893
10-20	26.214	3.641	2.718	2.573	1.845	3.689	2.961	2.524
20-30	53.592	17.185	7.767	1.699	2.427	5.291	2.621	2.524
30-40	71.699	8.058	14.078	3.835	4.660	13.786	11.942	6.311
40-50	22.330	4.126	3.981	1.214	0.825	3.592	4.029	1.602
50-60	16.893	2.330	2.816	1.068	0.437	3.010	4.126	0.922
60-70	10.583	0.680	1.845	0.728	0.631	2.087	2.913	0.485
70-80	8.981	0.728	1.165	0.971	0.583	1.602	2.670	0.437
80-90	6.068	0.388	0.534	0.777	0.534	1.019	1.990	0.340
90-100	6.068	0.291	0.291	0.388	0.874	1.650	1.602	0.388
100-110	4.417	0.097	0.146	0.194	0.971	0.777	1.311	0.291
110-120	4.369	0.097	0.146	0.388	1.408	1.311	0.680	0.340
120-130	3.932	0.243	0.000	0.097	1.359	0.631	1.311	0.243
130-140	3.738	0.146	0.049	0.097	1.893	0.583	0.728	0.146
140-150	3.641	0.243	0.049	0.194	1.602	0.874	0.631	0.049
150-160	2.767	0.097	0.194	0.049	1.553	0.583	0.243	0.000
160-170	2.184	0.049	0.243	0.000	1.359	0.291	0.243	0.000
170-180	1.796	0.146	0.000	0.000	0.874	0.291	0.534	0.000
180-190	0.825	0.049	0.000	0.097	0.291	0.097	0.243	0.000
190-200	1.019	0.049	0.000	0.049	0.437	0.243	0.243	0.000
200-210	0.728	0.049	0.000	0.000	0.388	0.049	0.243	0.000
210-220	0.777	0.049	0.000	0.049	0.291	0.243	0.194	0.000
220-230	0.680	0.000	0.000	0.049	0.388	0.000	0.194	0.000
230-240	0.583	0.000	0.049	0.000	0.194	0.049	0.291	0.000
240-250	0.194	0.000	0.000	0.000	0.097	0.049	0.049	0.000
250-260	0.340	0.000	0.000	0.000	0.243	0.097	0.000	0.000
260-270	0.243	0.000	0.000	0.097	0.097	0.000	0.000	0.000
270-280	0.340	0.000	0.000	0.097	0.097	0.146	0.000	0.000
280-290	0.146	0.000	0.000	0.000	0.000	0.097	0.049	0.000
290-300	0.340	0.000	0.000	0.194	0.049	0.000	0.097	0.000
300-310	0.146	0.000	0.000	0.000	0.146	0.000	0.000	0.000
310-320	0.243	0.000	0.000	0.049	0.194	0.000	0.000	0.000
320-330	0.194	0.000	0.000	0.049	0.000	0.049	0.097	0.000
330-340	0.000	0.000	0.000	0.000	0.000	0.000	0.000	0.000
340-350	0.146	0.000	0.000	0.000	0.146	0.000	0.000	0.000
350-360	0.146	0.000	0.000	0.000	0.146	0.000	0.000	0.000

360-370	0.194	0.000	0.000	0.049	0.146	0.049	0.000	0.000
370-380	0.097	0.000	0.000	0.000	0.049	0.000	0.049	0.000
380-390	0.146	0.000	0.000	0.000	0.097	0.000	0.049	0.000
390-400	0.146	0.000	0.000	0.000	0.146	0.000	0.000	0.000
400-410	0.243	0.000	0.000	0.000	0.243	0.000	0.000	0.000
410-420	0.000	0.000	0.000	0.000	0.000	0.000	0.000	0.000
420-430	0.194	0.000	0.000	0.000	0.146	0.097	0.049	0.000
430-440	0.097	0.000	0.000	0.000	0.049	0.000	0.049	0.000
440-450	0.097	0.000	0.000	0.049	0.000	0.000	0.049	0.000
450-460	0.000	0.000	0.000	0.000	0.000	0.000	0.000	0.000
460-470	0.049	0.000	0.000	0.000	0.049	0.000	0.000	0.000
470-480	0.146	0.000	0.000	0.000	0.097	0.049	0.049	0.000
480-490	0.049	0.000	0.000	0.000	0.000	0.049	0.000	0.000
490-500	0.243	0.000	0.000	0.000	0.194	0.000	0.049	0.000
500-510	0.000	0.000	0.000	0.000	0.000	0.000	0.000	0.000
510-520	0.291	0.000	0.000	0.146	0.097	0.000	0.049	0.000
520-530	0.534	0.000	0.000	0.049	0.291	0.000	0.194	0.000
530-540	0.631	0.000	0.000	0.146	0.291	0.000	0.194	0.000
540-550	0.388	0.000	0.000	0.097	0.194	0.000	0.097	0.000
550-560	0.291	0.000	0.000	0.000	0.243	0.000	0.049	0.000
560-570	0.146	0.000	0.000	0.049	0.000	0.049	0.049	0.000
570-580	0.922	0.000	0.000	0.146	0.291	0.000	0.485	0.000
580-590	0.437	0.000	0.049	0.049	0.243	0.000	0.097	0.000
590-600	0.583	0.000	0.000	0.097	0.146	0.000	0.340	0.000
600-610	0.583	0.000	0.000	0.049	0.049	0.000	0.485	0.000
610-620	0.583	0.000	0.000	0.097	0.000	0.000	0.437	0.000
620-630	0.146	0.000	0.000	0.000	0.000	0.000	0.146	0.000
630-640	0.291	0.000	0.000	0.097	0.097	0.000	0.097	0.000
640-650	0.291	0.000	0.000	0.000	0.194	0.000	0.049	0.000
650-660	0.097	0.000	0.000	0.000	0.097	0.000	0.000	0.000
660-670	0.049	0.000	0.000	0.000	0.049	0.000	0.000	0.000
670-680	0.049	0.000	0.000	0.000	0.000	0.000	0.049	0.000

Note. Seismicity rate values are in Earthquakes per year (EQ/y). Values in this table are plotted in Figures 3b, 4b, and 4c. Values are rounded to three decimal places.

4.2.1 Regional

The average yearly rate of events ≥ **M** 5.0 in the study region is approximately 318 EQ/y. Seismicity is most frequent at depths ≤ 40 km (Figure 3b), with a rate of ~54 EQ/y between 0-10 km, ~26 EQ/y between 10-20 km, ~54 EQ/y between 20-30 km, and ~72 EQ/y between 30-40 km. Seismicity rates between 50-300 km decay approximately exponentially from ~22 EQ/y to < 1 EQ/y following the equation $log_{10}(y) = log_{10}(42) - h/125$, ($R^2$=0.96), where y is the rate in EQ/y and h is the depth in km (Figure 3b). This result is consistent with global seismicity rate-depth distributions presented by Frohlich (2006) and Houston (2015), who show that seismicity worldwide decays exponentially between 50-300 km proportional to $log_{10}(y) \sim - h/120$.

Seismic gaps are present between 330-340 km, 410-420 km, 450-460 km and 500-510 km (Figure 3b). A small peak in seismicity is present near 410 km (~5 events per 20.6 years). Seismicity increases within the Mantle Transition Zone (MTZ), with the most prominent peaks ~1 EQ/y located between 510-560 km, 570-580 km, and 590-620 km. Seismic activity decreases near 660 km, and ceases between 670-680 km (Figure 3b). These trends remain consistent with global seismicity rates distributed with depth (Frohlich, 1989, 2006; Houston, 2015; Billen, 2020; Zhan, 2020).

4.2.2 Subregions

We divide the study area into seven approximately equal-area subregions (Figure 4a) based on the regional distribution of hypocenters (Figure 2a), subduction, and faulting (Figure 1) in order to investigate the diversity of seismicity-depth patterns. Figure 4b presents seismicity rates for western Indonesian subregions including NW Sumatra, SE Sumatra, and Java. Figure 4c presents seismicity rates for eastern Indonesian subregions including the Banda Sea, Sulawesi-Seram, Celebes Sea-Philippines, and West Papua. Seismicity rates for all subregions are similar to the regional average (Figure 3b) at depths ≤ 40 km, with peaks between 0-10 km, abrupt decreases between 10-20 km, and peaks between 20-40 km (Figures 4b-c). However, there is strong deviation between subregions at depths exceeding 40 km (Figures 4b-c).

NW Sumatra exhibits the highest seismicity rate of ~17 EQ/y between 20-30 km depth. Many of these earthquakes may be aftershocks of the 2004 Sumatra-Andaman event. SE Sumatra exhibits the most frequent seismicity between 30-40 km, while Java exhibits the most frequent seismicity between 0 and 10 km (Figure 4b). All three western subregions in Figure 4b exhibit a similar decrease in seismicity between ~40-120 km, deviating below 120 km. Seismic activity in NW Sumatra is sparse deeper than 120 km, with no activity beyond 230 km depth (Figure 4b). In contrast, seismicity in SE Sumatra extends to greater depths but is sparse, with large seismic gaps between 180-230 km and 250-580 km (Figure 4b). Deeper events become increasingly more frequent in Java, with seismicity extending to 640 km. Intermittent peaks within the MTZ in Java do not appear to coincide with the 410, 520, and 660 km phase boundaries (Figure 4b).

All eastern Indonesian subregions (Figure 4c) show the most frequent seismicity between 30-40 km, the greatest rate of 14 EQ/y being exhibited by the Celebes Sea-Philippines. As in western Indonesia, eastern subregions deviate with increasing depth. West Papua deviates

strongest from the other subregions, rapidly decreasing in seismicity deeper than 40 km with no seismicity beyond 150 km, similar to NW Sumatra (Figures 4b-c). The Celebes Sea-Philippines and Sulawesi-Seram regions exhibit a similar decrease between 40 km and 190 km, deviating deeper than 200 km (Figure 4c). In contrast, the Banda Sea decreases in seismicity rapidly between 40-60 km, and exhibits a broad seismicity peak of ~1-2 EQ/y between 100-190 km (Figure 4c). This broad peak is not present in any other subregion. Deep seismicity, particularly within the MTZ is most frequent in the Celebes Sea-Philippines, Banda Sea, and Sulawesi-Seram regions. The Banda Sea exhibits a peak at 410 km identical to the regional average (Figure 4c). Seismicity in the Banda Sea and Celebes Sea-Philippines comprises the majority of seismicity between 500 km to 680 km, extending to between 660-670 km and 670-680 km respectively.

The most significant observations regarding seismicity rates versus depth can be summarized as follows: (1) Seismicity is most frequent at depths ≤ 40 km. However, some of these events likely have default depths of 10 and 33 km automatically assigned and may therefore be poorly resolved; (2) The regional seismicity rate decreases exponentially between 50-300 km at a rate consistent with the global distribution (Houston, 2015); (3) Seismicity gaps are observed for all subregions at intermediate-deep depths; (4) The deepest events in Indonesia, ≥ 670 km depth, only occur in the Banda Sea and Celebes Sea-Philippines; (5) Seismicity rates deeper than 300 km decrease westward until no seismicity is evident beneath NW Sumatra, with the exception of West Papua; (6) Elevated seismicity between 100 and 200 km is only present in the Banda Sea, implying a distinct process or boundary not evident in other subregions; And (7) the most frequent MTZ seismicity is located in the Banda Sea and Celebes Sea-Philippines, where seismicity peaks at 410 km and variably between 520-660 km imply that the 410, 520 and 660 km phase boundaries may play a significant role in increasing upper mantle seismicity. While there are several factors that contribute to intraslab seismicity, phase transitions at these boundaries increase viscous resistance of the mantle to the motion of subducting slabs (Zhan, 2020). Increased mantle resistance contributes to increased strain rates and therefore elevated intraslab seismicity as slabs pass through the MTZ (Billen, 2020; Zhan, 2020).

4.3 Cross-Sections of Intermediate and Deep Seismicity

Intermediate seismicity is defined as events occurring between 70 – 300 km depth, with deep events ≥ 300 km depth, together forming inclined Wadati-Benioff zones that reflect

deformation within subducting slabs (Frohlich, 2006; Houston, 2015; Zhan, 2020). Wadati-Benioff zones can extend to the upper boundary of the lower mantle, typically terminating near 660 km at the deepest, with some special cases extending tens of km deeper into the lower mantle (e.g. Tonga-Kermadec subduction; Frohlich, 1989; Billen, 2020). Intermediate and deep earthquakes account for approximately 20% and 3% of recent Indonesian seismicity respectively (Table 1). Figure 5a displays the distribution of intermediate and deep earthquakes throughout Indonesia at depths ≥ 70 km. As observed with seismicity rates previously, the majority of intermediate and deep seismicity occurs in eastern Indonesia (Figures 4b-c), decreasing in abundance west of 120˚E, with deep events ceasing north of ~1˚S in Sumatra (~100˚E; Figure 5a). To greater analyze these trends and their associations with Indonesian tectonics, we plot 2D cross-sections and 3D profiles for (1) the Molucca Sea, Celebes Sea, and southern Philippines (Cross-sections AA' and BB'); (2) Sulawesi island (Cross-section CC'); (3) West Papua (Cross-sections DD' and EE'); (4) the Banda Sea (Cross-section FF'); (5) Java (Cross-sections GG', HH', and II'); and (6) Sumatra (Cross-sections JJ', KK', and LL'). Cross-section locations are presented in Figure 5b.

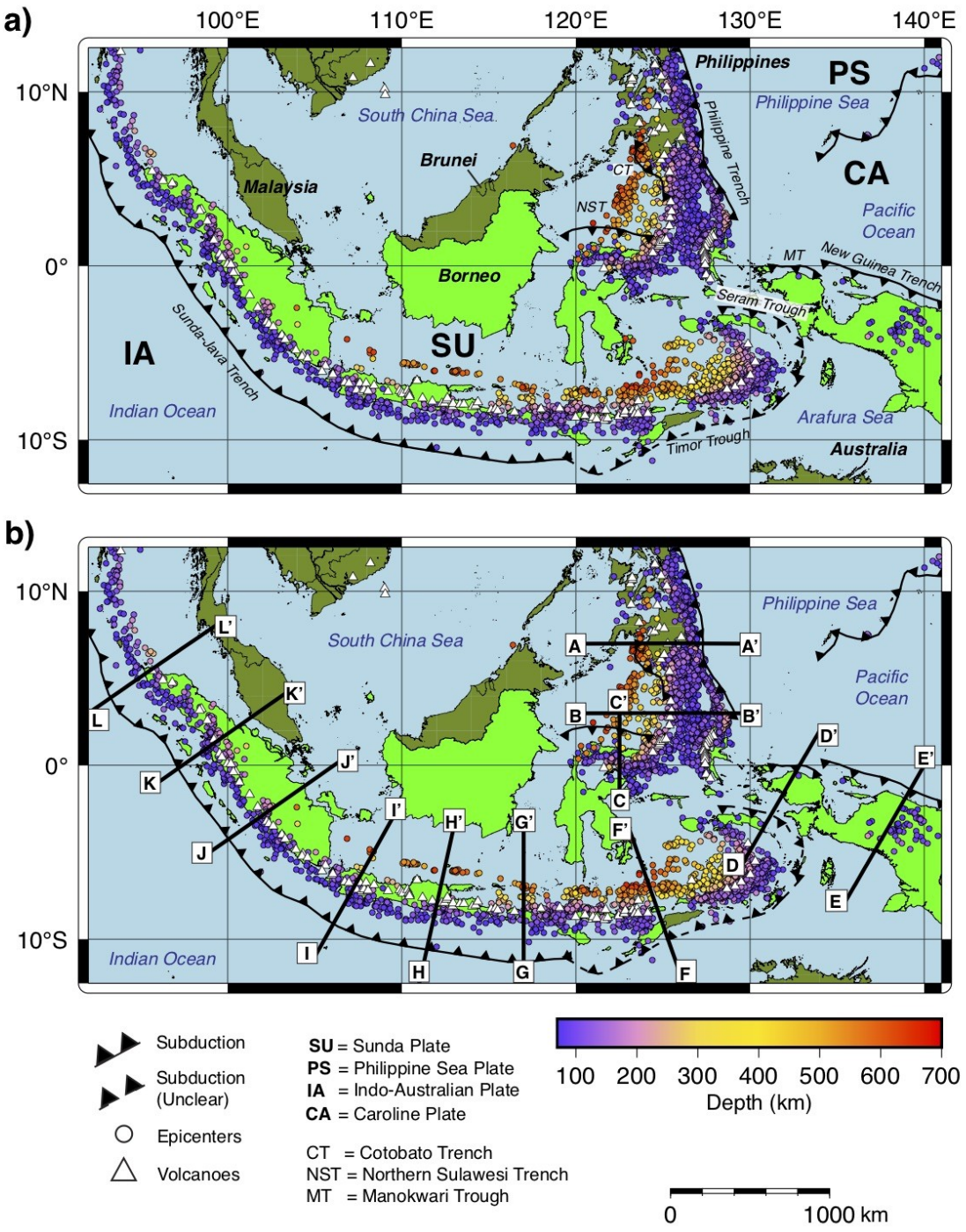

Figure 5. (a) Seismicity of Indonesia and neighboring regions ≥ 70 km depth for events ≥ **M** 4.6 between January 1, 2000 and July 28, 2020. Intermediate and deep earthquakes are most common in east Indonesia (east of 120˚E), decreasing westward toward Sumatra. Deep events are not evident north of 1˚S in Sumatra. Subduction zone boundaries are obtained from Hall (2012), Patria and Hall (2017), and Hall (2018). (b) Cross-section lines. Each section line is 1000

km long, except for CC' which is 500 km long. Hypocenters are projected from within 50 km on either side of each section line and all are scaled 1:1.

4.3.1 Molucca Sea-Celebes Sea-Philippines

Figure 6a presents the seismicity of the Molucca Sea, Celebes Sea, and the southern Philippines in map view, with Figures 6b-d showing 3D seismicity profiles and cross-sections. Hypocenters gradually increase in depth westward beneath the Celebes Sea and Mindanao to a depth of 678 km (Figures 6a-d), and abruptly eastward to ~250 km beneath Halmahera island (Figure 6a-c). Viewed in 3D (Figure 6b), intermediate and deep seismicity is consistent with the inverted U-shaped Wadati-Benioff zones of the subducted Molucca Sea plate beneath the continuing arc-arc collision in the Molucca Sea Collision Zone (MSCZ) active since ~2 Ma (Figure 6a; Silver and Moore, 1978; Cardwell et al., 1980; Moore and Silver, 1983; Hall, 1987; Widiwijayanti et al., 2004; Hall and Spakman, 2015; Fan and Zhao, 2018).

The Molucca Sea plate is comprised of two opposite-dipping slabs, the Sangihe slab dipping beneath the Sunda plate in the west, and the Halmahera slab dipping beneath the Philippine Sea plate in the east (Figures 6a-b; Bird, 2003; Hall and Spakman, 2015). The Sangihe slab exhibits a greater along-strike length than the Halmahera slab, trending S-N from Sulawesi to Mindanao while the Halmahera slab is constrained primarily beneath northern Halmahera island (Figures 6a-b). Figure 6c shows the Wadati-Benioff zones of the Sangihe, Philippine Sea and Cotobato slabs beneath Mindanao, where arc-arc collision is essentially complete (~7°N; Widiwijayanti et al., 2004; Hayes, 2018). The Sangihe slab at this location is largely aseismic, exhibiting a seismic gap between ~200-540 km, with dense seismicity between ~540-680 km (Figures 6b-c; Hall and Spakman, 2015; Fan and Zhao, 2018). The cause of this seismic gap is not clear from available literature. The Philippine Sea slab exhibits a similar orientation as the Sangihe slab and is seismically active to ~250 km, estimated to represent young subduction beginning ~5 Ma (Lallemand et al., 1998; Hall and Spakman, 2015; Hall, 2018). However, recent tomography modeling by Fan and Zhao (2018) imaged the Philippine Sea slab extending aseismically to ~450-600 km depth near Mindanao, implying subduction in the southern Philippine trench is older than originally believed and likely initiated around the same time as the Sangihe slab (~20-25 Ma; Hall and Spakman, 2015; Fan and Zhao, 2018; Hall, 2018). Conversely, the Cotobato slab, dipping moderately eastward (Hayes, 2018) and seismically

active to < 100 km depth has been considered a younger feature, with the Wadati-Benioff zone likely representative of the extent of subduction (Figure 6c; Cardwell et al., 1980; Fan and Zhao, 2018; Hall, 2018).

Farther south (~3˚N), where arc-arc collision remains active (Widiwijayanti et al., 2004), Figure 6d shows the Wadati-Beniof zone of the Halmahera slab dipping steeply eastward, with the Sangihe slab exhibiting a moderate dip compared to Figure 6c. These orientations are consistent with recent tomography modeling and the orientation of the Molucca Sea plate (Hall and Spakman, 2015; Fan and Zhao, 2018). The Halmahera slab is estimated to have initiated subduction ~10 Ma (Hall and Spakman, 2015). The southern extent of the Philippine Sea slab is present east of the Halmahera slab at this location to ~100 km depth (Figure 6d; Hayes, 2018). The tomography models of Fan and Zhao (2018) indicate the Philippine Sea slab may extend to ~300 km depth at this location, exhibiting an overturned-to-the-east dip and possibly interacting with the Halmahera slab, though this remains unclear from seismicity.

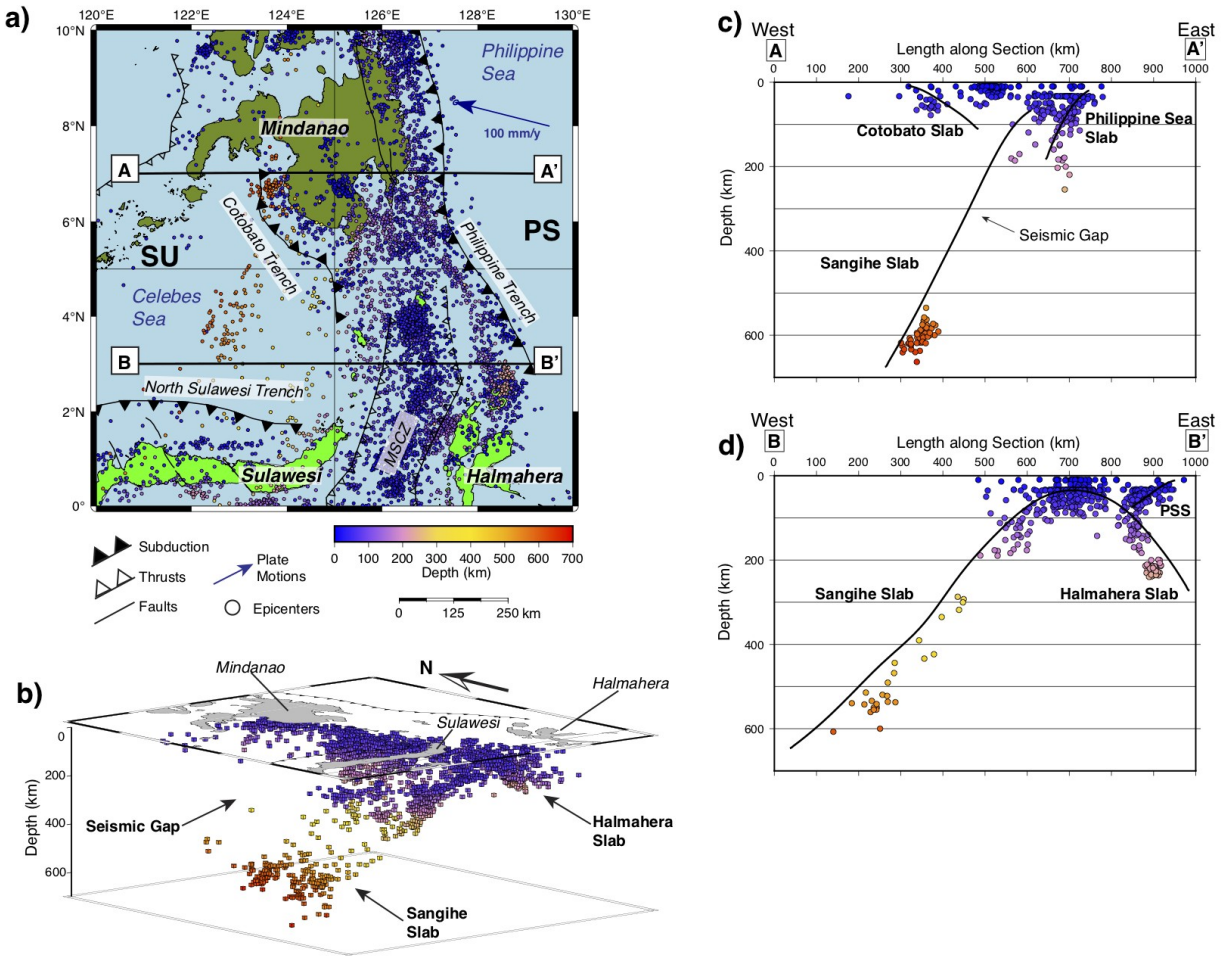

Figure 6. (a) Seismicity of the Molucca Sea, Celebes Sea and southern Philippines region for all events ≥ **M** 4.6 between January 1, 2000 and July 28, 2020. Indonesia is highlighted in green. Intermediate and deep hypocenters are observed primarily beneath Halmahera island and the Celebes Sea. SU = Sunda plate, and PS = Philippine Sea plate. Plate velocities are with respect to the Sunda plate obtained from the MORVEL velocity model (DeMets et al., 2010). Faults and boundaries are obtained from Moore and Silver (1983), Widiwijayanti et al. (2004), Besana and Ando (2005), Watkinson et al. (2011), Hall (2012), Tsutsumi and Perez (2013), Watkinson and Hall (2017), and Hall (2018). (b) 3D seismicity profile for events ≥ 70 km, looking NE at the subducted U-shaped Molucca Sea plate (Sangihe and Halmahera slabs). Map area is the same as panel (a). (c) Cross-section AA', looking north beneath Mindanao. The Sangihe slab dips westward to ~660 km with a prominent seismic gap. (d) Cross-section BB', looking north beneath the Molucca Sea Collision Zone (MSCZ). The inverted U-shaped Molucca Sea plate is clearly visible. PSS = Philippine Sea slab. Slab 2.0 predictions (Hayes, 2018) are plotted as thick black lines for all cross-sections and scaling is 1:1.

4.3.2 Sulawesi

Figure 7a displays the seismicity of Sulawesi, and Figure 7b displays a N-S cross-section through the Northern Sulawesi trench. At the trench, the subduction of Celebes Sea oceanic lithosphere beneath the island is clearly defined (Figures 7a-b; Silver et al., 1983a; Hall and Spakman, 2015). Hypocenters gradually increase in depth south of the trench beneath the Gulf of Tomini, defining the Wadati-Benioff zone of the Celebes slab, as referred to by Hall and Spakman (2015) (Figures 7a-b). Hypocenters deviate from Slab 2.0 (Hayes, 2018) near ~150 km depth and extend to ~300 km depth (Figure 7b). Deeper hypocenters are likely representative of the nearby Sangihe slab (Figures 6a, 6d, and 7a). Seismicity indicates subduction of the Celebes slab is deepest in the east and shallows westward, forming a wedge-shape that has been imaged with tomography (Figure 7a; Hall and Spakman, 2015; Hall, 2018).

South of the Celebes slab is a steeply north-dipping, poorly defined Wadati-Benioff zone seismically active to near 200 km depth, tentatively termed the Sula slab by Hall and Spakman (2015) (Figure 7b). Hall and Spakman (2015) suggest that the Sula slab is a remnant of older subduction at the East Arm of the island that ceased ~20 Ma, and that the majority of the slab has since detached near 200 km depth and descended aseismically into the mantle. The current steep

dip is a likely result of slab interactions with the Celebes and Sangihe slabs, with lithospheric delamination a likely contributor to current seismicity (Hall and Spakman, 2015).

In addition to active subduction at the Northern Sulawesi trench, Bird (2003) suggested that the east-dipping Makassar thrust (sometimes labeled as a trench; Valkaniotis et al., 2018) on Sulawesi's western coast may represent early subduction development due to the presence of hypocenters ~70 km depth beneath the interior of the island (Figure 7c). Figure 7c exhibits a cross-section through the Makassar thrust, where hypocenters are located beneath the estimated depth of the continental crust the in this region (~35 km; Hall et al., 2009). However, there is no Wadati-Benioff zone present, and no recent tomography or gravity models confirm or deny the presence of a developing slab (Hall et al., 2009).

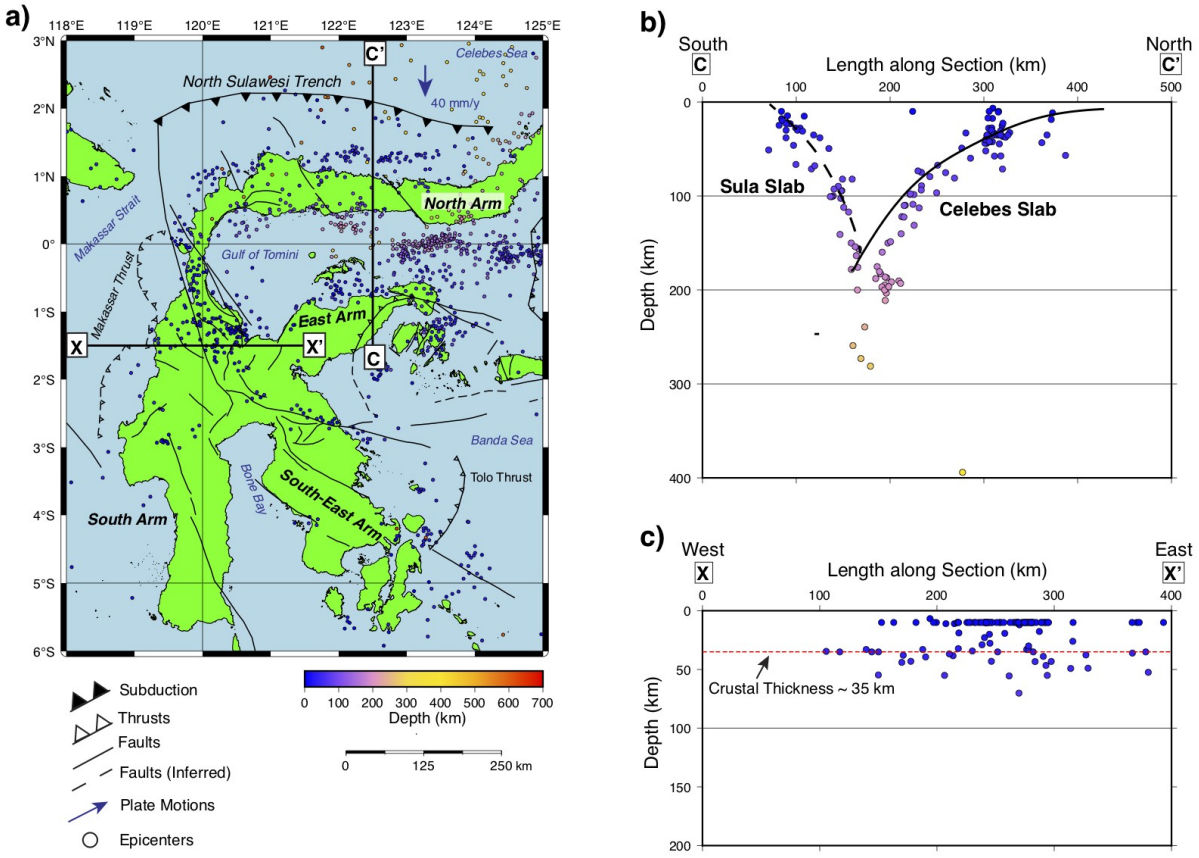

Figure 7. (a) Seismicity of Sulawesi for all events ≥ **M** 4.6 between January 1, 2000 and July 28, 2020. Intermediate and deep seismicity is concentrated south of the Northern Sulawesi trench beneath the Gulf of Tomini. Deeper seismicity to the north below the Celebes Sea is due to the presence of the Sangihe slab (Figure 6). Faults and boundaries are obtained from Silver et al. (1983a), Cipta et al. (2016), Watkinson and Hall (2017), Hall (2018), Nugraha and Hall (2018),

and Valkaniotis et al. (2018). Relative motion of the Celebes Sea at the Northern Sulawesi trench is obtained from GPS estimates (Gómez et al., 2000; Bock et al., 2003). (b) Cross-section CC' looking west beneath northern Sulawesi. The Celebes slab dips to the south and is clearly defined to ~300 km. The Sula slab is a likely remnant of older subduction prior to subduction of the Celebes slab. Slab 2.0 predictions (Hayes, 2018) are plotted as thick black lines. Slab 2.0 geometry for the Sula slab is not available (Hayes, 2018), and is therefore estimated using the dashed black line based on Hall and Spakman (2015). Scaling is 1:1. (c) Cross-section XX' through the Makassar thrust, looking north. Some hypocenters clearly lie below the estimated thickness of the continental crust but no Wadati-Benioff zone is visible. Note that this cross-section is supplementary and is not presented in Figure 5b so as to avoid crowding. The approximate thickness of the continental crust is indicated by the dashed red line (Hall et al., 2009). Scaling is 1:1.

4.3.3 West Papua

Figure 8a displays the seismicity of West Papua in map view, and Figures 8b-c illustrate two cross sections through the island. The Caroline plate subducts at the New Guinea trench (Tregoning and Gorbatov, 2004) and a smaller developing subduction zone at the Manokwari trough north of the Bird's Head (Figure 8a; Milsom et al., 1992; Baldwin et al., 2012; Hall, 2014; Hall, 2018). Hypocenters gradually increase in depth southward beneath the interior of the island, with activity deeper than 100 km not evident west of ~136˚E toward the Bird's Head (Figure 8a). Hypocenters in Figure 8b extend to ~100 km depth at the Manokwari trough, with a separate Wadati-Benioff zone extending to ~300 km depth beneath Seram related to subduction beneath the Banda Sea (Hall and Spakman, 2015). Figure 8c shows a poorly defined, southward-dipping Wadati-Benioff zone to 200 km depth beneath the interior of West Papua. A flat slab orientation is observed in Figure 8c (Hayes, 2018), consistent with Tregoning and Gorbatov (2004) who imaged the subducting Caroline plate dipping southward between 10˚- 30˚ to ~300 km depth. Shallow seismicity observed above the slab in Figure 8c may represent activity on several thrust faults that cross the interior of the island (Baldwin et al., 2012; Watkinson and Hall, 2017).

Slab 2.0 predicts the slab to extend the entire length of the New Guinea trench (Hayes, 2018), but the nature of current subduction remains debated (Baldwin et al., 2012). The

484 westward decrease in seismic activity observed in Figure 8a may be related to buoyant
485 lithosphere from active seafloor spreading at the Ayu trough, and oblique convergence between
486 the Pacific (Caroline and Philippine Sea) and Indo-Australian plates (Figure 8a; Fujiwara et al.,
487 1995; Bock et al., 2003; Baldwin et al., 2012). The age of the Caroline plate decreases westward
488 from 25 Ma near 136˚E to 0 Ma at the Ayu trough (Figure 8a; Seton et al., 2020). Additionally,
489 the Pacific and Indo-Australian plates (Figure 8a) exhibit an approximate convergence angle of
490 ~70˚NE (Hinschberger et al., 2005), producing a significant sinistral lateral component
491 accommodated by E-W trending fault zones such as the Sorong fault (Figure 8a; Watkinson and
492 Hall, 2017). These factors likely impede subduction at the western New Guinea trench and
493 similarly at the Manokwari trough, which in addition to being a young feature resides nearest to
494 active spreading at the Ayu trough (Figure 8a; Milsom et al., 1992; Hall, 2014). The nature of the
495 flat slab subduction observed in Figure 8c however is not clear and poorly documented in
496 available literature, requiring further investigation beyond the scope of this paper.

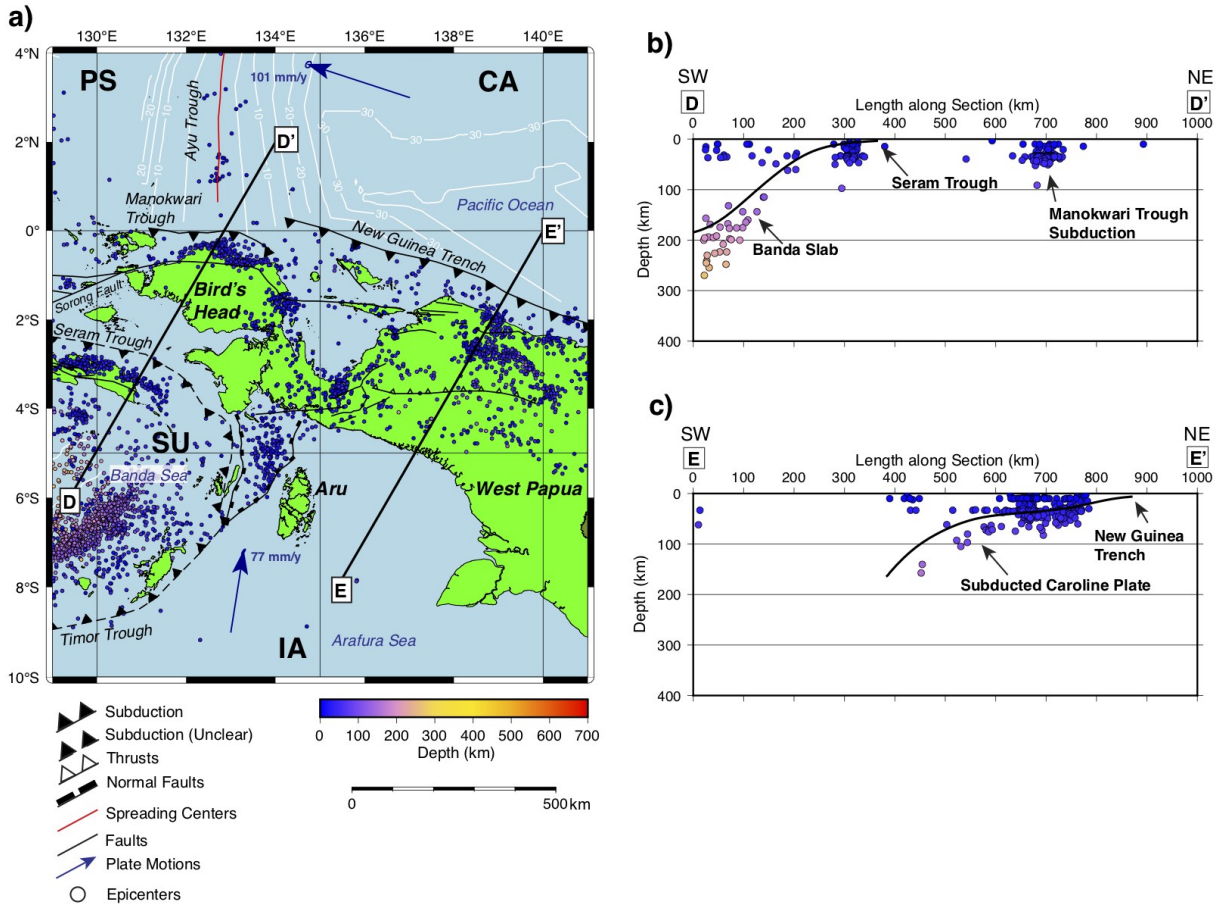

497

Figure 8. (a) Seismicity of West Papua for all events ≥ **M** 4.6 between January 1, 2000 and July 28, 2020. Indonesia is highlighted in green. Intermediate seismicity decreases westward toward the Bird's Head as the age of the lithosphere of the Caroline plate decreases toward the Ayu trough. Convergence between the Indo-Australian and Caroline plates is oblique with a ~70˚NE convergence angle (Hinschberger et al., 2005). Seafloor age contours (Seton et al., 2020) are shown as white lines with C.I. = 5 Ma. SU = Sunda plate, PS = Philippine Sea plate, CA = Caroline plate, and IA = Indo-Australian plate. Plate velocities are obtained from the MORVEL velocity model (DeMets et al., 2010) with respect to the Sunda plate. Faults and boundaries are obtained from Saputra et al. (2014), Adhitama et al. (2017), Patria and Hall (2017), and Watkinson and Hall (2017). (b) Cross-section DD' looking NW beneath the Bird's Head and Seram. Subduction at the Manokwari trough is poorly developed, and no Slab 2.0 (Hayes, 2018) geometry is available for the Manokwari trough subduction. Seismicity at the Seram trough is related to the subduction of the Banda slab (Hall and Spakman, 2015). (c) Cross-section EE' looking NW through West Papua. A flat slab orientation is visible with little seismicity at the trench. Slab 2.0 predictions (Hayes, 2018) for all cross-sections are plotted as thick dark lines and scaling is 1:1.

4.3.4 Banda Sea

The seismicity of the Banda Sea is presented in map view in Figure 9a, with cross sections and 3D plots presented in Figures 9b-d. The Banda Sea exhibits a unique distribution of hypocenters inboard of the Timor and Seram troughs that form the 180˚ curved collisional boundary between the Indo-Australian and Sunda plates (Figure 9a; Charlton, 2000; Hinschberger et al., 2005; Spakman and Hall, 2010; Hall and Spakman, 2015). Hypocenters in Figures 9b-d define a highly deformed, curved Wadati-Benioff zone dipping northward at the Timor trough and southward at the Seram trough. Hypocenters highlight a slab with a gently west-plunging synformal fold that is flat between 600-660 km depth (Hayes, 2018), consistent with tomography models (Spakman and Hall, 2010; Widiyantoro et al., 2011b; Hall and Spakman, 2015). A prevailing theory suggests this lithospheric folding is a result of rollback of a single slab termed the Banda slab into a curved Jurassic embayment on the Australian continental margin beginning ~10-15 Ma (Charlton, 2000; Spakman and Hall, 2010; Audley-Charles, 2011; Hall and Spakman, 2015).

528 The current nature of subduction within the Banda Sea remains controversial. Many
529 studies indicate that subduction ceased following the arrival of Australian continental crust at the
530 Timor and Seram troughs ~2 Ma, switching tectonics from active subduction to collision and
531 accretion (Bird, 2003; Hinschberger et al., 2005; Audley-Charles, 2011; Patria and Hall, 2017;
532 Hall, 2018). The Timor and Seram troughs are commonly interpreted as foreland basins rather
533 than active marine trenches, and GPS velocities suggest the majority of convergence near Timor
534 is transferred to back-arc thrusts such as the Wetar thrust (Figures 9a and 9d; Bock et al., 2003;
535 Spakman and Hall, 2010; Audley-Charles, 2011; Patria and Hall, 2017). Despite this, it is likely
536 that a significant amount of continental subduction has occurred. Tate et al. (2015) quantified
537 215-229 km of continental subduction beneath Timor using balanced cross-sections, where
538 others (Hinschberger et al., 2005; Harris, 2011) indicate that as much as 400 km of continental
539 subduction has occurred based on tomography and geochemical evidence.
540 Spakman and Hall (2010) proposed that lithospheric delamination may be an important
541 mechanism that accommodates the continuing rollback and folding of the Banda slab, which may
542 make it possible for subduction to continue beneath the active collision zone where continental
543 subduction is becoming increasingly difficult (Harris, 2011). In addition, slab tearing beneath
544 Seram and Timor has been proposed from tomography and seismic gaps beneath the islands
545 (Figures 9b-d; Widiyantoro et al., 2011b), consistent with the final stages of subduction and
546 suggesting that subduction of the Banda slab is in the later stage prior to break-off and descent
547 into the mantle (Wortel and Spakman, 2000; Harris, 2011; Widiyantoro et al., 2011b; Hall and
548 Spakman, 2015). Regardless, the Banda slab remains a prevalent source of deep seismicity
549 beneath the Banda Sea.

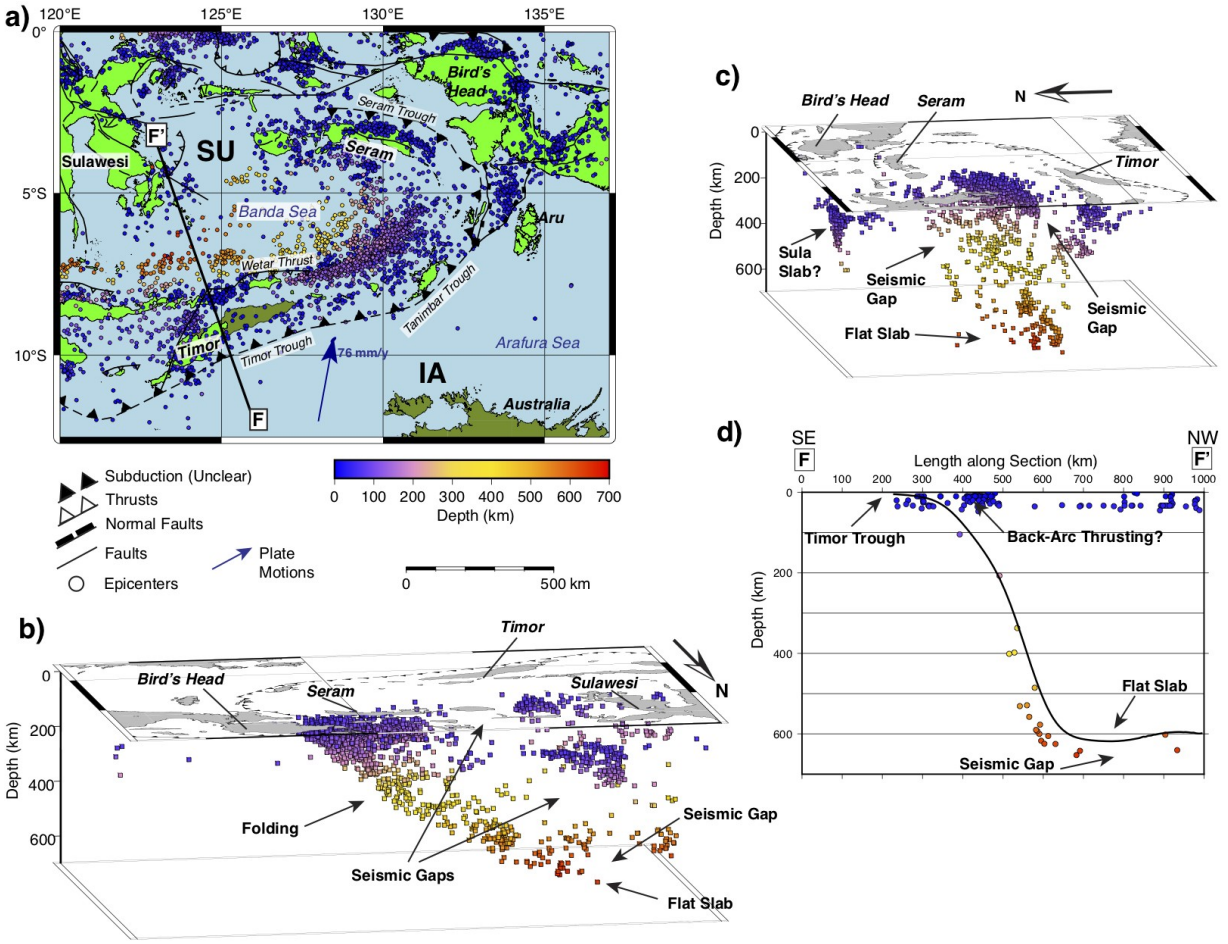

Figure 9. (a) Seismicity of the Banda Sea region for all events ≥ **M** 4.6 between January 1, 2000 and July 28, 2020. Indonesia is highlighted in green. Intermediate and deep seismicity is concentrated inboard of the Timor and Seram troughs that form the collisional boundary between the Indo-Australian and Sunda plates. SU = Sunda plate, and IA = Indo-Australian plate. Plate velocities are obtained from the MORVEL velocity model (DeMets et al., 2010) with respect to the Sunda plate. Faults and boundaries are obtained from Silver et al. (1983b), Roosmawati and Harris (2009), Watkinson et al. (2011), Saputra et al. (2014), Cipta et al. (2016), Koulali et al. (2016), Adhitama et al. (2017), Patria and Hall (2017), Watkinson and Hall (2017), Hall (2018), Nugraha and Hall (2018), and Valkaniotis et al. (2018). (b) 3D seismicity profile for events ≥ 70 km depth, looking south at the folded Banda slab. Several seismic gaps are present and may be related to slab tearing (Widiyantoro et al., 2011b). Map area is the same as panel (a). (c) 3D seismicity profile for events ≥ 70 km depth, looking SE at the folded Banda slab. Several seismic gaps and flat slab orientation near 600-600 km are visible. Map area is the same as panel (a). (d)

Cross-section FF' looking SW beneath Timor. The slab is traceable with seismicity to below 600 km, where a flat slab orientation is observed between 600-660 km. Upper plate seismicity is likely due to back-arc thrusting on the Wetar thrust. Slab 2.0 predictions (Hayes, 2018) for all cross-sections are plotted as thick dark lines and scaling is 1:1.

4.3.5 Java

The seismicity of Java and the surrounding islands is displayed in map view in Figure 10a, with cross-sections presented in Figures 10b-d. Subduction of the Indo-Australian plate beneath the Sunda plate at the Sunda-Java trench is clearly visible (Figure 10a). Hypocenters extend to ~660 km beneath Java, highlighting a steeply north-dipping slab consistent with tomography models (Figures 10a-d; Widiyantoro et al., 2011a; Hall and Spakman, 2015). At this location, relatively old lithosphere between 100 - 155 Ma (Jacob et al., 2014; Seton et al., 2020) subducts with a ~7-15˚E convergence angle (Figures 10b-c; Hall and Spakman, 2015). Nearly direct convergence and lithospheric age may contribute to the observed steep dip (Hall and Spakman, 2015).

Notable changes in seismicity are observed in cross-sections across Java (Figures 10b-d). East of Java (Figure 10b) hypocenters form a relatively continuous Wadati-Benioff zone to ~660 km depth, with shallower seismicity in the upper plate likely related to back-arc thrusting along the Flores thrust (Figure 10a). In contrast, hypocenters beneath eastern Java (Figure 10c) exhibit a prominent seismic gap from approximately 150 – 600 km depth, with seismicity resuming below 600 km. This gap has been proposed to correspond with a hole in the slab that extends for ~400 km laterally beneath east Java as imaged by tomography (Widiyantoro et al., 2011a; Hall and Spakman, 2015; Dokht et al., 2018). Beneath west Java (Figure 10d) this gap is no longer visible, with the Wadati-Benioff zone relatively continuous to ~200 km, and intermittent between 200-660 km. In all cross-sections, the majority of seismicity appears to lie below the Slab 2.0 estimate for the slab top (Hayes, 2018), suggesting seismicity is primarily within the slab rather than the overlying plate or at the plate interface (Figures 10b-d).

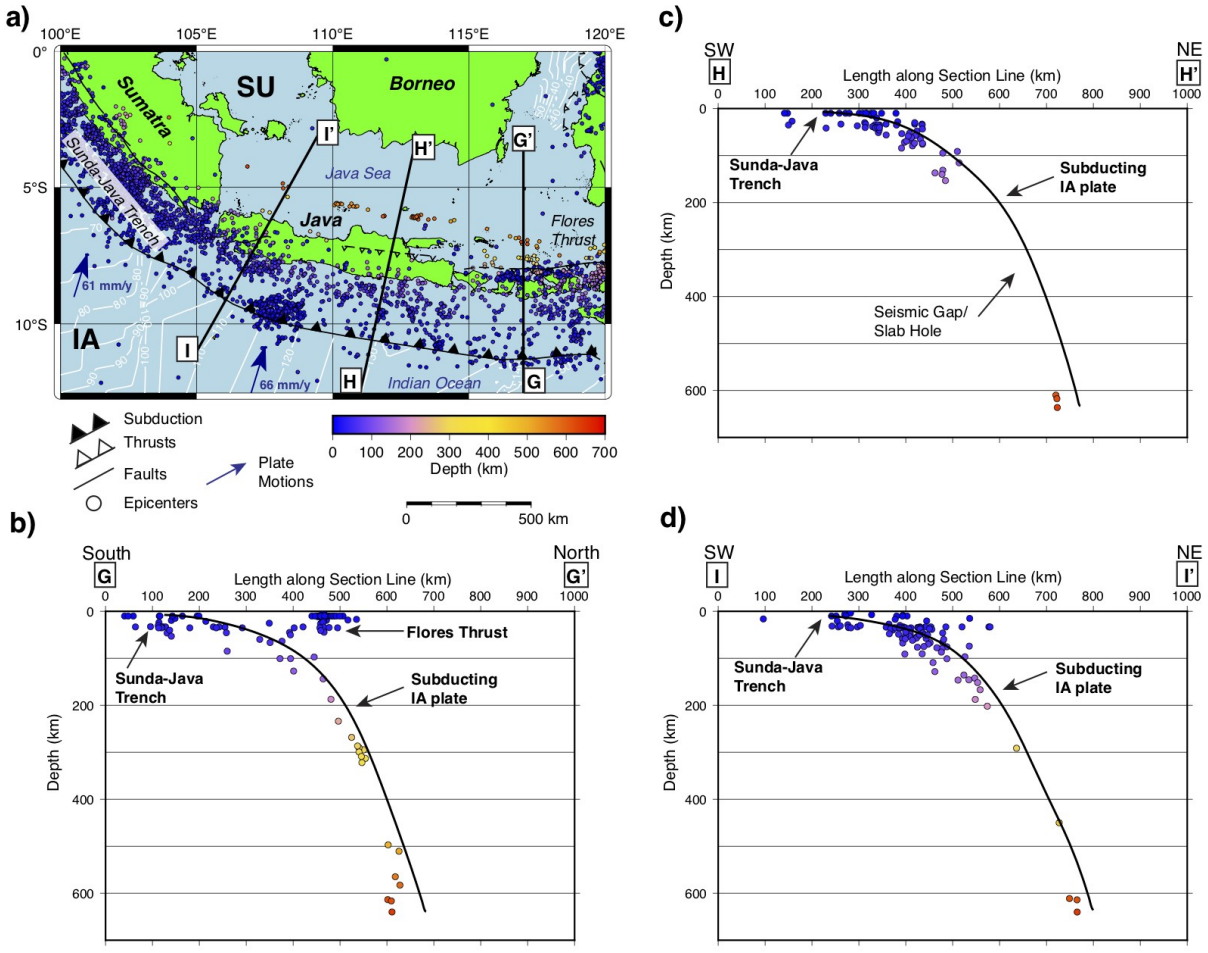

Figure 10. (a) Seismicity of Java and surrounding islands for all events ≥ **M** 4.6 between January 1, 2000 and July 28, 2020. Indonesia is highlighted in green. The Indo-Australian slab subducts northward beneath the Sunda plate, and deep seismicity decreases westward toward Sumatra. White lines are seafloor age contours (Seton et al., 2020) with C.I. = 5 Ma. SU = Sunda plate, and IA = Indo-Australian plate. Plate velocities are with respect to the Sunda plate obtained from the MORVEL velocity model (DeMets et al., 2010). Faults and boundaries are obtained from Silver et al. (1983b), Hall (2012), Koulali et al. (2016), and Supendi et al. (2018). (b) Cross-section GG' looking west beneath the islands east of Java. The Wadati-Benioff zone is nearly continuous, with upper plate seismicity likely related to back-arc thrusting on the Flores thrust. (c) Cross-section HH' looking NW beneath eastern Java. A large seismic gap is present and has been linked to a hole in the slab imaged by tomography (Widiyantoro et al., 2011a; Hall and Spakman, 2015). (d) Cross-section II' looking NW through western Java. The gap observed in section HH' is no longer visible. All cross-sections show minimal activity in the upper plate and

near the predicted plate interface. Slab 2.0 predictions (Hayes, 2018) for all cross-sections are plotted as thick dark lines and scaling is 1:1.

4.3.6 Sumatra

The seismicity of Sumatra is displayed in Figure 11a, with cross-sections presented in Figures 11b-d. North of ~1˚S, hypocenters occur no deeper than ~250 km (Figures 4b, 11a and 11c; Hayes, 2018). Slab material however has been imaged with seismic tomography to depths of at least 660 km throughout the majority of Sumatra (Widiyantoro et al., 2011; Hall and Spakman, 2015). Figure 11b shows that in southeastern Sumatra, seismicity traces a relatively continuous and steeply dipping Wadati-Benioff zone active to ~250 km, with Slab 2.0 predicting the slab extends aseismically to near 600 km (Hayes, 2018). In contrast, Figure 11c in central Sumatra near 1˚N exhibits a more shallow-dipping Wadati-Benioff zone to ~200 km, with Slab 2.0 predictions extending no further than 250 km depth (Hayes, 2018). A similar dip is observed in NW Sumatra near 5˚N (Figure 11d), but the Wadati-Benioff zone is poorly defined to ~200 km. The majority of seismicity in Figure 11d appears clustered around the predicted shallow plate interface, suggestive of increased megathrust activity following the 2004 $\mathbf{M}_w$ 9.1 Sumatran-Andaman earthquake (Lay et al., 2005). Additionally, Figure 11e illustrates slight dip changes between Figures 11c and 11d predicted by Slab 2.0 (Hayes, 2018), which are noted and proposed to coincide with a N-S trending tear in the slab located between ~1-5˚ N by Hall and Spakman (2015).

The observed changes in subduction geometry and lack of deep seismicity moving NW from Java to Sumatra may be due to increasing oblique convergence, decreasing lithospheric age and increasing mantle temperatures (Widiyantoro and van der Hilst, 1996; Saita et al., 2002; McCaffrey, 2009; Hall and Spakman, 2015). The western Sunda-Java trench is a partitioned subduction zone, where oblique convergence is divided between the trench and trench-parallel strike-slip faults in the upper plate such as the Sumatran fault (Figure 11a; McCaffrey, 2009). Convergence angles between the Indo-Australian and Sunda plates are estimated to change from below 20˚ in southern Sumatra to near 30˚ in northern Sumatra, producing a significant dextral lateral component (Baroux et al., 2002; Bock et al., 2003; McCaffrey, 2009). Clusters of shallow seismicity inboard of the trench in Figures 11b-d may reflect motion on the Sumatran fault.

633 The age of the subducting lithosphere varies considerably along-strike, related to extinct
634 seafloor spreading in the Wharton Basin (Indian Ocean; Jacob et al., 2014; Hall and Spakman,
635 2015; Seton et al., 2020). Ages range from ~100 Ma at the oldest in southern Sumatra to ~35 Ma
636 at the youngest near the equator, and increase to ~70 Ma near 5˚N (Figure 11a; Jacob et al.,
637 2014; Seton et al., 2020). The changes in slab orientations in Figures 11b-d are a likely due to
638 increasingly buoyant lithosphere and a decreasing direct convergent component impeding
639 subduction. In addition, NW Sumatra has been determined to exhibit an abnormally thin MTZ
640 and depressed 410 km phase boundary, indicating the mantle is warmer than average, a likely
641 result of mantle upwelling through slab tears (Saita et al., 2002; Kong et al., 2020). Deep
642 earthquake generation is highly dependent on temperature, and where temperatures are too great
643 slabs will resort to ductile deformation (Houston, 2015). Mantle temperatures increase between
644 Java and Sumatra as deep seismicity decreases, suggesting temperature is a primary control on
645 deep seismicity beneath Sumatra (Figure 11a; Saita et al., 2002; Kong et al., 2020).

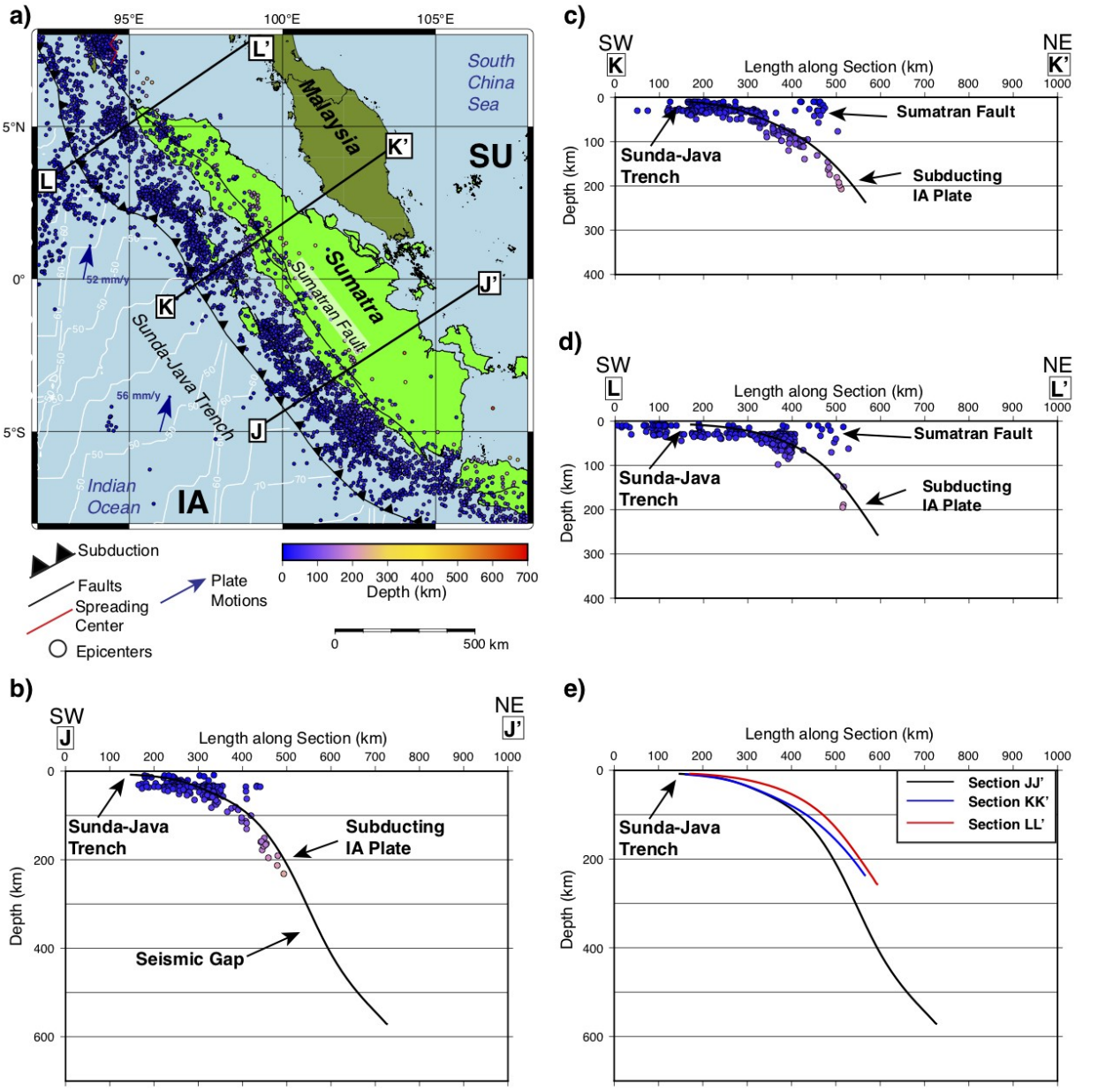

Figure 11. (a) Seismicity of Sumatra for all events ≥ **M** 4.6 between January 1, 2000 and July 28, 2020. Indonesia is highlighted in green. Deep seismicity disappears north of ~1˚S. Convergence becomes more oblique to the NW, and lithospheric ages decrease to ~35 Ma near the equator and increase again farther north. White lines are seafloor age contours (Seton et al., 2020) with C.I. = 5 Ma . SU = Sunda plate, and IA = Indo-Australian plate. Plate velocities are with respect to the Sunda plate obtained from the MORVEL velocity model (DeMets et al., 2010). Faults and boundaries are obtained from Hall (2012), Mukti et al. (2012), and Omang et al. (2016). (b) Cross-section JJ' looking NW through southern Sumatra. The Wadati-Benioff zone terminates

near 250 km depth though Slab 2.0 (Hayes, 2018) extends to ~600 km. (c) Cross-section KK' looking NW through central Sumatra. The slab exhibits a slightly shallower dip than section JJ', with majority of seismicity appearing present within the slab. Upper plate seismicity clusters are likely related to movement on the Sumatran fault. (d) Cross-section LL' looking NW through northern Sumatra. Seismicity appears concentrated at the plate interface and within the slab. Upper plate seismicity clusters are likely related to movement on the Sumatran fault. Slab 2.0 predictions (Hayes, 2018) for all cross-sections are plotted as thick dark lines and scaling is 1:1. (e) Direct comparison of Slab 2.0 orientations (Hayes, 2018) in Figures 11b-d to illustrate slab dip changes. Hall and Spakman (2015) suggest a N-S trending tear in the slab is located between 1-5˚ N, (between cross-sections KK' and LL'), which corresponds to slight dip changes between these cross-sections. Subducting lithosphere at section LL' is older than at section KK' (Seton et al., 2020). Scaling is 1:1.

4.3.7 Intraslab Mechanisms

Intraslab earthquakes are similar in many respects to shallow crustal events, but occur at much higher temperatures and pressures and by different mechanisms including slab flexure, metamorphic dehydration, thermal shear instability, and mineral phase transitions (Houston, 2015; Romeo and Álvarez-Gómez, 2018; Billen, 2020; Zhan, 2020). Figure 12 shows that intraslab focal mechanisms in Indonesia are quite heterogeneous. Thermomechanical models expect events ≥ 400 km to be down-dip compressional (reverse faulting) and intermediate events to be down-dip tensional (normal faulting; Houston, 2015). Indonesian slabs appear to deviate from this prediction however, with normal faulting mechanisms commonly observed for events ≥ 300 km, and reverse and oblique mechanisms common at intermediate depths (Figure 12). Though unclear, this deviation may be related to a number of factors, including slab age, subduction rates, strain heterogeneity, and inherited faults within the slab (Wiseman et al., 2012; Houston, 2015; Billen, 2020). Intraslab events can reach magnitudes ≥ **M** 7.0, and particularly those that occur at shallower depths can pose serious seismic hazards. One such example is the 2009 $\mathbf{M}_w$ 7.6 Padang event, which occurred ~ 80 km depth (Wiseman et al., 2012).

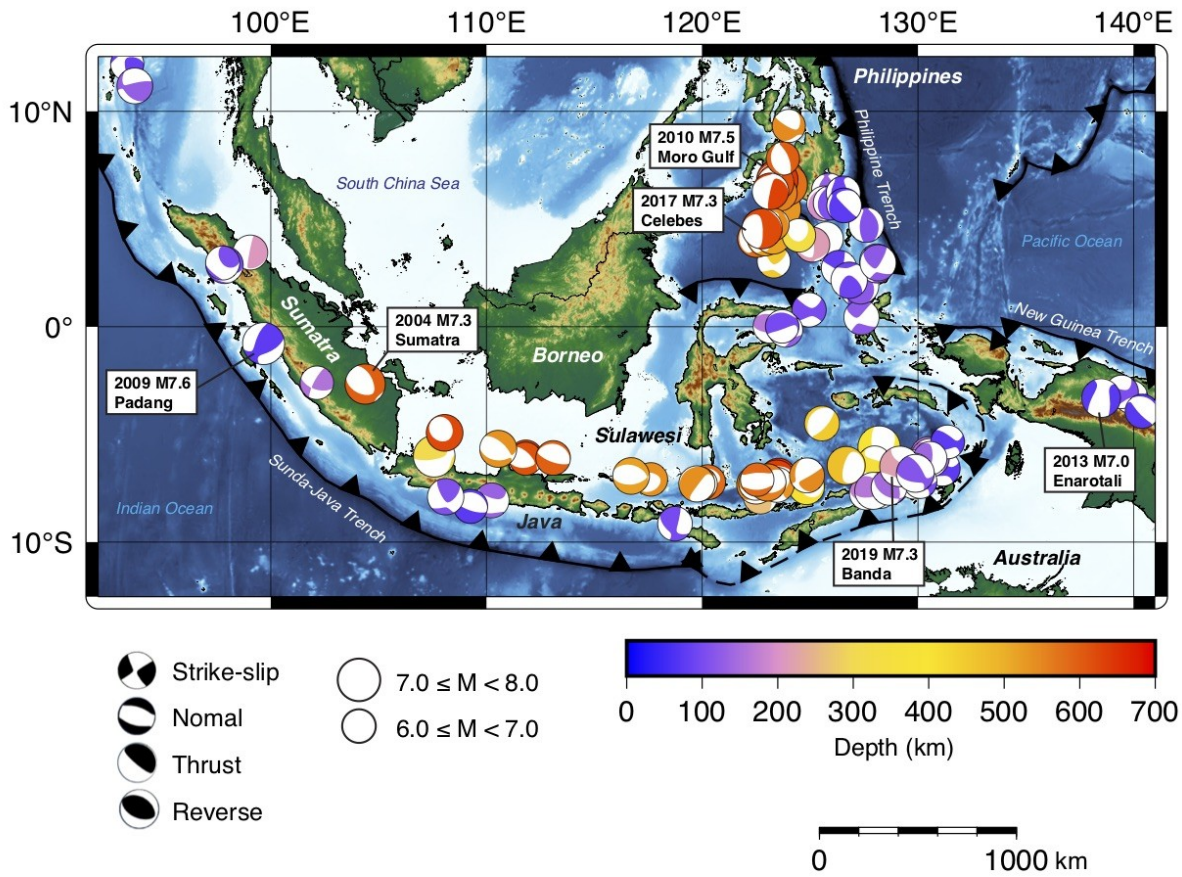

682

683 *Figure 12.* Intermediate and deep GCMT focal mechanisms for events ≥ **M** 6.0 and ≥ 70 km
684 depth between January 1, 2000 and July 28, 2020. Mechanisms are scaled by magnitude and
685 colored by depth. Notable events are labeled (refer to Table 3). Focal mechanisms are diverse,
686 with normal faulting common for deep earthquakes and oblique mechanisms common for
687 intermediate earthquakes.

688 4.4 Shallow Seismicity and Focal Mechanisms

689 In contrast to intermediate and deep seismicity, shallow seismicity ≤ 70 km depth is more
690 representative of plate motions and associated deformation nearest to the surface, accounting for
691 the majority of seismicity in Indonesia (~77%; Table 1; Figure 2a). Shallow events pose a greater
692 seismic hazard than deeper events due to hypocenter locations close to the surface (Table 3).
693 Sources of shallow seismicity in Indonesia are diverse, but for ease of organization, the primary
694 sources are defined as (1) megathrust, (2) crustal, and (3) shallow intraslab.

695 4.4.1 Megathrusts

Megathrusts define the shallow plate interface (≤ 50 km depth) between subducting and overriding plates, behaving as large-scale thrust faults that accommodate plate convergence at subduction zones (Kanamori, 1986; Bilek and Lay, 2018). Able to generate the largest earthquakes recorded by modern instrumentation (~**M** 9.0), megathrust events are often associated with destructive ground shaking and tsunamis, creating serious seismic hazards (Polet and Kanamori, 2000; Bilek and Lay, 2018). Several subduction zones in Indonesia host active megathrusts, the most prominent being the Sunda megathrust within the Sunda-Java trench (Figures 13 and 14).

The Sunda megathrust is most active offshore of Sumatra (Figure 13), where abundant shallow thrust faulting mechanisms ≥ **M** 5.0 within the forearc support a megathrust interface with an average NW strike and shallow NE dip (Figure 13a). Much of this elevated seismicity is likely related to stress changes following the December 2004 $\mathbf{M}_w$ 9.1 Sumatra-Andaman event (Figure 13b; Lay et al., 2005). The Sunda megathrust is a prevalent source of seismic hazard for Sumatra, and since the destructive 2004 earthquake has produced several ≥ **M** 7.0 events including the 2005 $\mathbf{M}_w$ 8.6 Nias, and the 2007 $\mathbf{M}_w$ 8.4 Bengkulu-Mentawai events (Figure 13b; Table 3; Hughes et al., 2010; Hayes et al., 2017). In Java however, megathrust activity appears more subdued, with fewer events than Sumatra ≥ **M** 5.0 supporting a north-dipping thrust interface (Figure 14a), very few events ≥ **M** 6.0 (Figure 14b), and no great earthquakes known to have occurred in at least a century (Newcomb and McCann, 1987; Okal, 2012). The largest recent event was a $\mathbf{M}_w$ 7.7 SW of Java on July 17, 2006 (Figure 14b; Table 3; Hayes et al., 2017). Irsyam et al. (2020) indicate that this lack of notable megathrust events implies interplate coupling on the Sunda megathrust is much lower in Java than in Sumatra. However, Hanifa et al. (2014) interpret a locked megathrust from GPS measurements of coastal uplift and contraction in western Java, and Widiyantoro et al. (2020) identify seismic gaps between 20-30 km depth south of Java as likely locations of future ruptures. Though no great magnitude megathrust events have been recorded near Java, such a rupture may be possible (Okal, 2012). Hanifa et al. (2014) estimate a moment accumulation of $\mathbf{M}_w$ 8.7 over the past three centuries in west Java, assuming tectonic stress is not periodically released by slow slip. Regardless, the damage caused by the 2006 $\mathbf{M}_w$ 7.7 Java earthquake and tsunami and tsunamigenic deposits identified on Java's southern coast indicate the Sunda megathrust remains a notable source of seismic hazard for Java (Hayes et al., 2017; Irsyam et al., 2020; Widiyantoro et al., 2020).

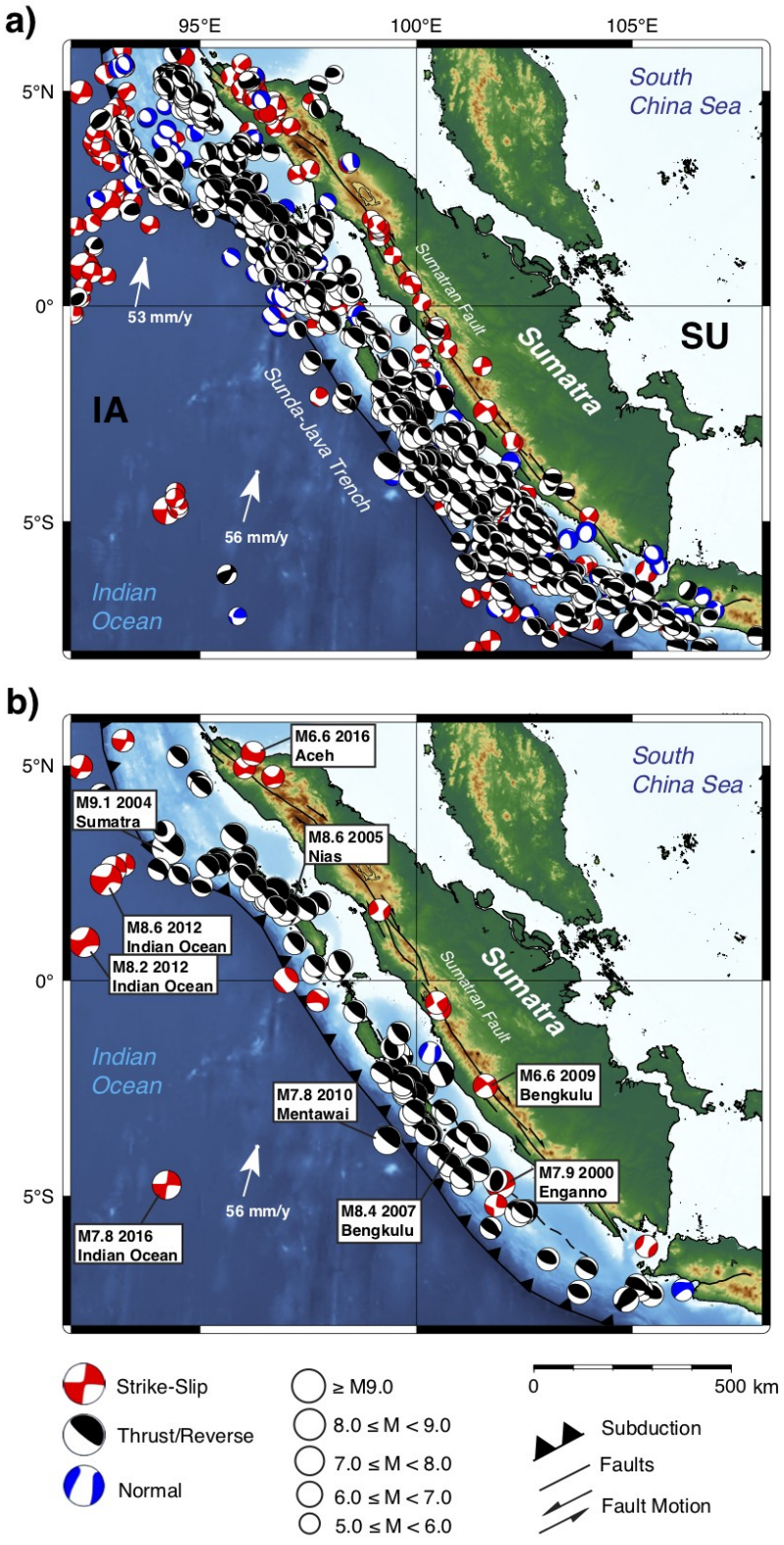

727

728 *Figure 13.* Shallow GCMT focal mechanisms ≤ 70 km for Sumatra between January 1, 2000 and

729 July 28, 2020 for (a) events ≥ **M** 5.0 and (b) events ≥ **M** 6.0. Events are colored by mechanism

730 and scaled by magnitude. Thrusting is abundant, supporting a NE-dipping megathrust at the
731 Sunda-Java trench. Strike-slip faulting is primarily concentrated along the Sumatran fault and
732 along N-S trending faults within the Indian Ocean. Notable events in panel (b**)** are presented in
733 Table 3. Faults and boundaries are obtained from Hall (2012), Mukti et al. (2012), Omang et al.
734 (2016), and Supendi et al. (2018). White arrows are plate velocity vectors obtained with respect
735 to the Sunda plate from the MORVEL velocity model (DeMets et al., 2010). SU = Sunda plate,
736 and IA = Indo-Australian plate.

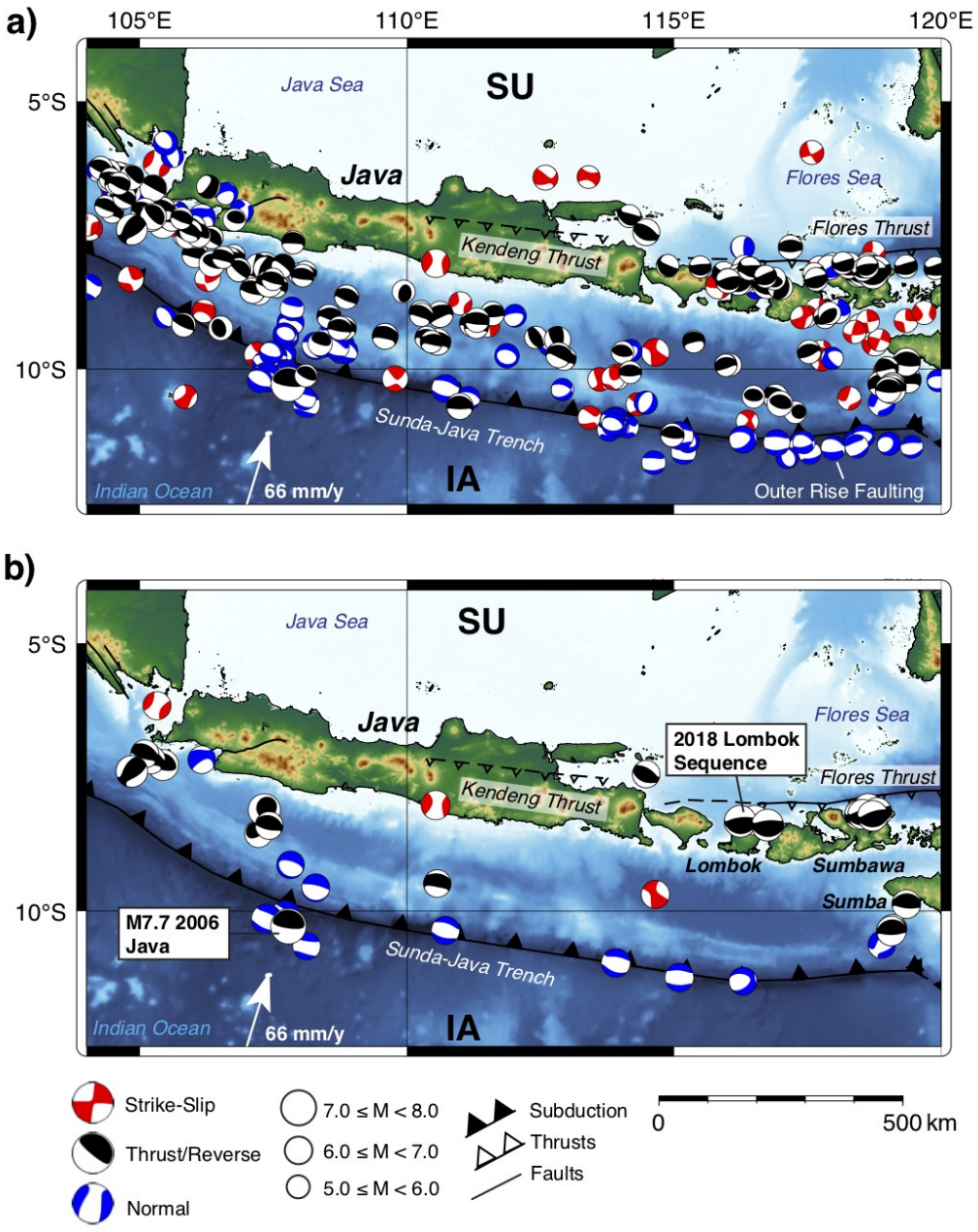

737

Figure 14. Shallow GCMT focal mechanisms ≤ 70 km for Java between January 1, 2000 and July 28, 2020 for (a) events ≥ **M** 5.0 and (b) events ≥ **M** 6.0. Events are colored by mechanism and scaled by magnitude. Thrusting mechanisms are less abundant along the Sunda-Java trench in Java than in Sumatra, likely indicating low coupling on the megathrust (Irsyam et al., 2020). Other thrust mechanisms are located along the Flores back-arc thrust. Normal faulting in the outer-rise of the trench indicates down-dip extension and low megathrust coupling (Christensen and Ruff, 1988). Notable events in panel (b) are presented in Table 3. Faults and boundaries are obtained from Silver et al. (1983b), Hall (2012), Koulali et al. (2016), Supendi et al. (2018). White arrows are plate velocity vectors obtained with respect to the Sunda plate from the MORVEL velocity model (DeMets et al., 2010). SU = Sunda plate, and IA = Indo-Australian plate.

Megathrusts in eastern Indonesia are not as large or active as the Sunda megathrust, but are nonetheless notable sources of seismicity. The Northern Sulawesi trench for example (Figure 15) produced a destructive $\mathbf{M}_w$ 7.4 event in November 2008 (Figure 15; Table 3), the latest of several ≥ **M** 7.0 events since 1990 including a $\mathbf{M}_w$ 7.8 in 1990, a $\mathbf{M}_w$ 7.5 and $\mathbf{M}_w$ 7.0 in 1991, a $\mathbf{M}_w$ 7.9 and $\mathbf{M}_w$ 7.0 in 1996, and a $\mathbf{M}_w$ 7.0 in 1997 (Gómez et al., 2000; Hayes et al., 2017; U.S. Geological Survey, 2020). Though the 2008 **M** 7.4 earthquake is the only event ≥ **M** 6.0 that has occurred in the trench since January 2000, based on past events a future ≥ **M** 7.0 rupture is likely, with the trench designated by others as a serious seismic hazard (Cipta et al., 2016; Irsyam et al., 2020).

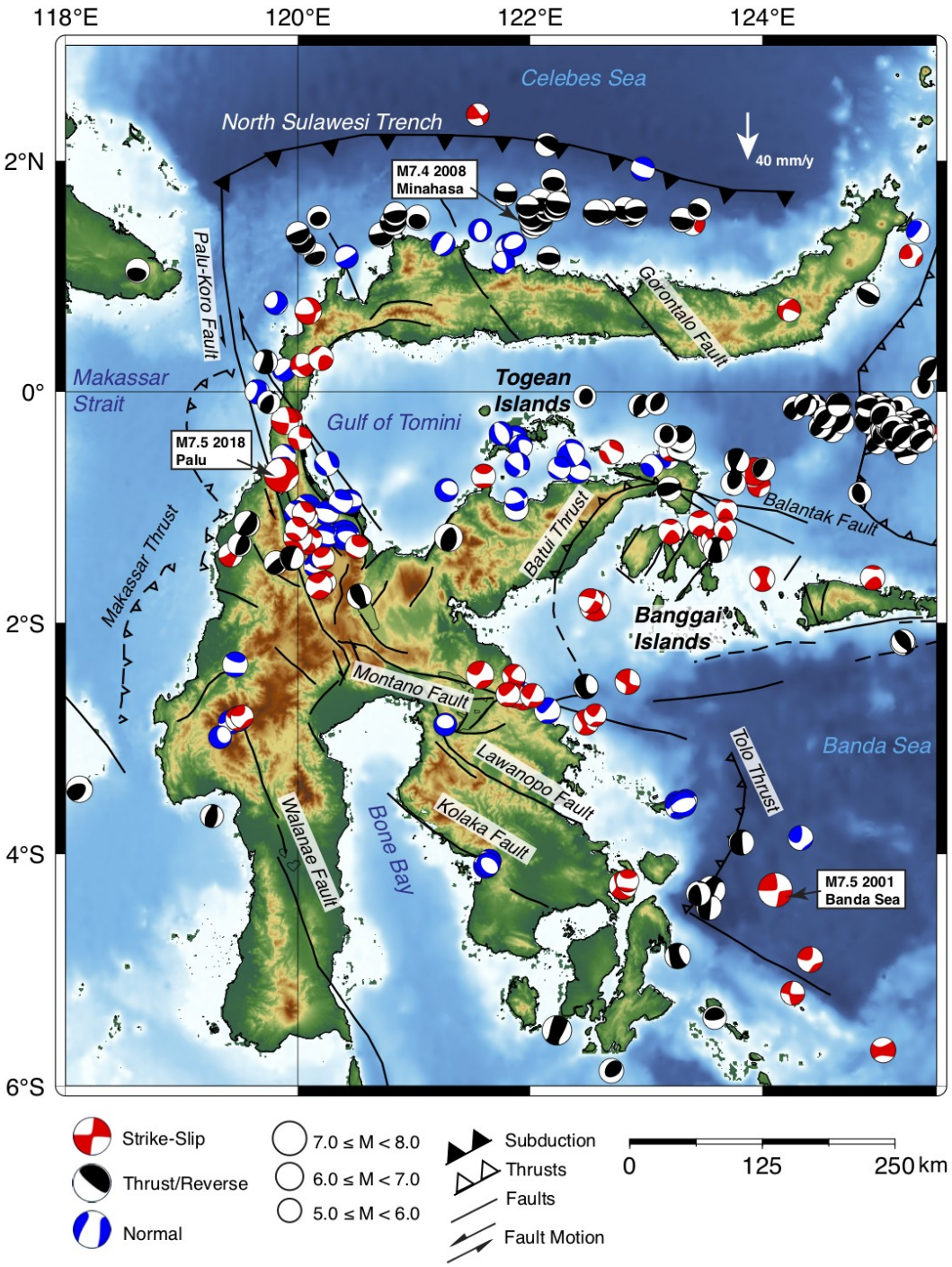

Figure 15. Shallow GCMT focal mechanisms ≤ 70 km depth for Sulawesi between January 1, 2000 and July 28, 2020 for events ≥ **M** 5.0. Events are colored by mechanism and scaled by magnitude. Subduction is active in the North Sulawesi trench, with strike-slip mechanisms supporting E-W sinistral slip along the Palu-Koro and Montano faults. Strike-slip motion is present in the Banggai islands. Other faults do not exhibit notable seismic activity but are likely

764 tectonically active (Soquet et al., 2006; Watkinson and Hall, 2017). Normal faulting is present
765 throughout the Gulf of Tomini, associated with rollback of the Celebes slab (Hall and Spakman,
766 2015; Watkinson and Hall, 2017). Faults and boundaries are obtained from Silver et al. (1983a),
767 Hall (2012), Cipta et al. (2016), Watkinson and Hall (2017), Hall (2018), Nugraha and Hall
768 (2018), and Valkaniotis et al. (2018). White arrows are relative motion velocity vectors of the
769 Celebes Sea obtained from GPS (Gómez et al., 2000; Bock et al., 2003). Notable events are
770 labeled and presented in Table 3.

771 The western New Guinea trench exhibits less-frequent seismicity than other megathrusts
772 in Indonesia (Figure 16), and the nature of subduction remains debated (Baldwin et al., 2012).
773 No thrust events ≥ **M** 6.0 since January 2000 are evident within the western New Guinea trench
774 (Figure 16b), though some events < **M** 6.0 do support a shallow southward-dipping thrust
775 interface primarily near 138˚E (Figure 16a). Despite exhibiting low seismicity, the New Guinea
776 trench is capable of generating great magnitude events, the most recent being the February 1996
777 $\mathbf{M}_w$ 8.2 Biak earthquake (Okal, 1999; Henry and Das, 2002). Another similar event in 1914 is
778 speculated to have occurred near the 1996 rupture (Okal, 1999), suggesting the trench is often
779 seismically locked and prone to infrequent great magnitude ruptures. A possible explanation is
780 that though the trench is active, it may not absorb all of the estimated ~70 mm/y of convergence
781 (Tregoning and Gorbatov, 2004) between the Indo-Australian and Caroline plates, with fold and
782 thrust belts on the interior of the island providing additional accommodation (Bock et al., 2003;
783 Tregoning and Gorbatov, 2004; Hinschberger et al., 2005). The majority of recent active
784 thrusting activity appears clustered to the west in the Manokwari trough, which exhibits
785 abundant thrust mechanisms ≥ **M** 5.0 supportive of a SSW-dipping thrust interface and
786 southward subduction (Figure 16a; Hall, 2014). Two ≥ **M** 7.0 thrust events occurred near the
787 trough in 2009, a $\mathbf{M}_w$ 7.7, and a $\mathbf{M}_w$ 7.4, and seven events **M** 6.0-7.0 occurred between 2000 –
788 2009, suggesting the Manokwari trough is an active megathrust and a notable seismic hazard,
789 despite being a developing subduction zone (Figure 16b; Hall, 2014).

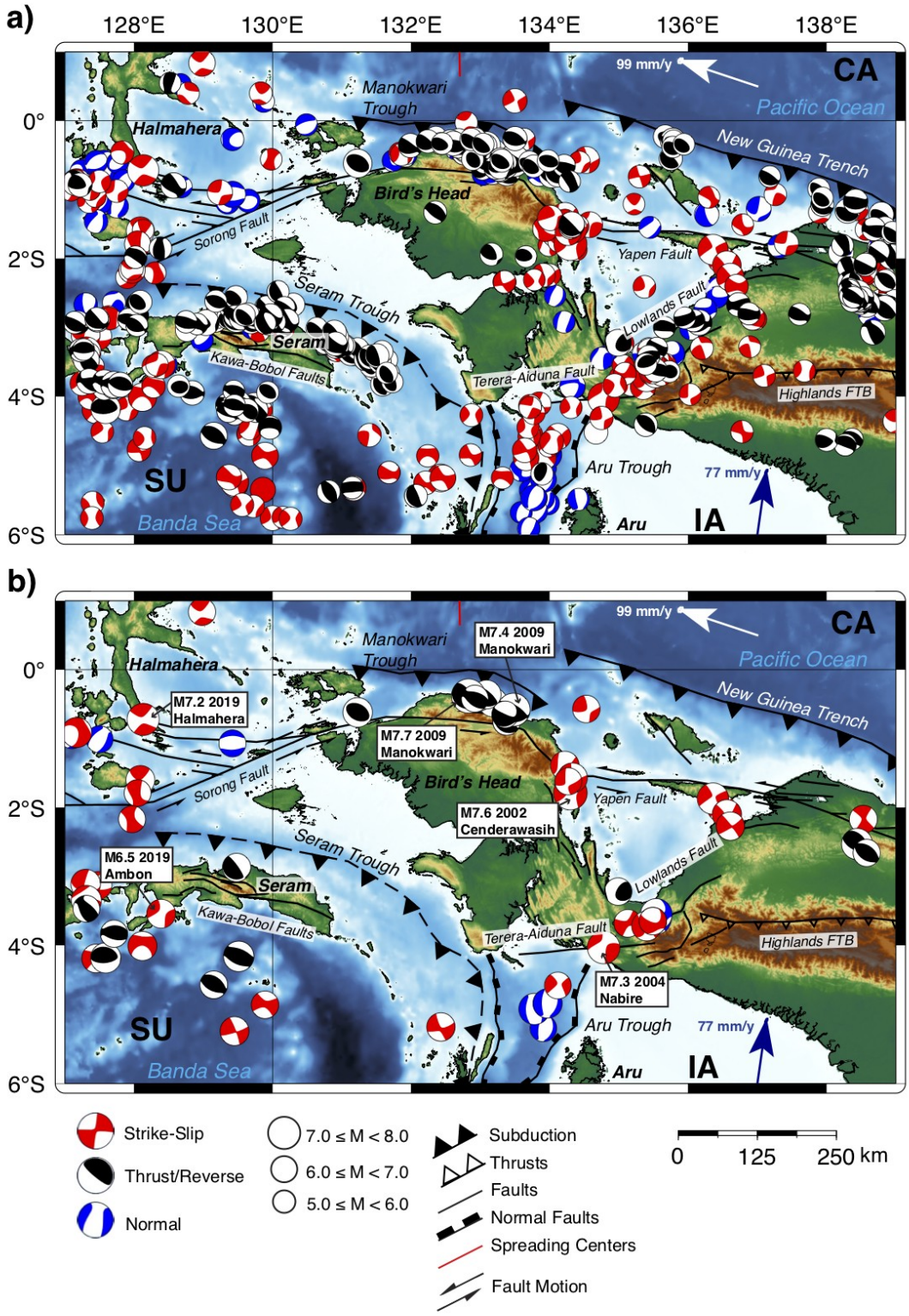

Figure 16. Shallow GCMT focal mechanisms ≤ 70 km depth for West Papua and Seram between January 1, 2000 and July 28, 2020 for (a) events ≥ **M** 5.0 and (b) events ≥ **M** 6.0. Events are colored by mechanism and scaled by magnitude. The western New Guinea trench exhibits little

to no seismic activity. Lithospheric age and oblique convergence may contribute to this. Strike-slip mechanisms supporting E-W sinistral shear are evident along the Yapen, Lowland, Terera-Aiduna, and western Sorong faults. Broad sinistral shear is transferred from the Terera-Aiduna fault to the western Sorong fault across Seram (Patria and Hall, 2017; Watkinson and Hall, 2017). Normal faulting is active in the Aru trough, associated with rollback of the Banda slab (Spakman and Hall, 2010; Adhitama et al., 2017). Notable events labeled in panel (b) are presented in Table 3. Faults and boundaries are obtained from Saputra et al. (2014), Adhitama et al. (2017), Patria and Hall (2017), Watkinson and Hall (2017), and Hall (2018). White and dark blue arrows represent plate velocities with respect to the Sunda plate obtained from the MORVEL plate velocity model (DeMets et al., 2010). SU = Sunda plate, CA = Caroline plate, and IA= Indo-Australian plate.

Megathrusting within the southern Philippine trench (Figure 17) appears most active near the Philippine island of Mindanao with abundant focal mechanisms < **M** 6.0 supportive of a west-dipping thrust interface (Figure 17a). Activity is not as abundant farther south near the Indonesian island of Morotai where the trench terminates (Figure 17a; Hall, 2018). Very few events ≥ **M** 6.0 are evident within the trench (Figure 17b), and a great magnitude event has not occurred within or near the trench east of Mindanao since ~1972 (U.S. Geological Survey, 2020). Few events ≥ **M** 7.0 have been characterized along the trench since ~1600, with such activity occurring primarily south of ~9˚N (Ye et al., 2012). In 2012, a $\mathbf{M}_w$ 7.6 thrust event occurred in the outer-rise east of the Philippine trench in a region of low megathrust activity (Figure 17b; Table 3), suggesting strain accumulation in the oceanic crust due to strong coupling on the megathrust (Christensen and Ruff, 1988; Ye et al., 2012). It is not currently understood however if a large megathrust event can be expected in the near future as a result.

Conversely, the Cotobato trench SW of Mindanao has produced several notable megathrust events in the past century. Several shallow focal mechanisms inboard of the trench ≥ **M** 5.0 support an ENE-dipping thrust interface with three events exceeding **M** 6.0, the largest being a $\mathbf{M}_w$ 7.5 in 2002 (Figure 17; Hayes et al., 2017). The trench also produced the destructive ~$\mathbf{M}_s$ 7.8 Moro Gulf earthquake and tsunami of 1976, with another likely similar event ~$\mathbf{M}_s$ 8.0 occurring in 1918, making the Cotobato trench a notable source of seismic hazard in the Celebes Sea region (Stewart and Cohn, 1979).

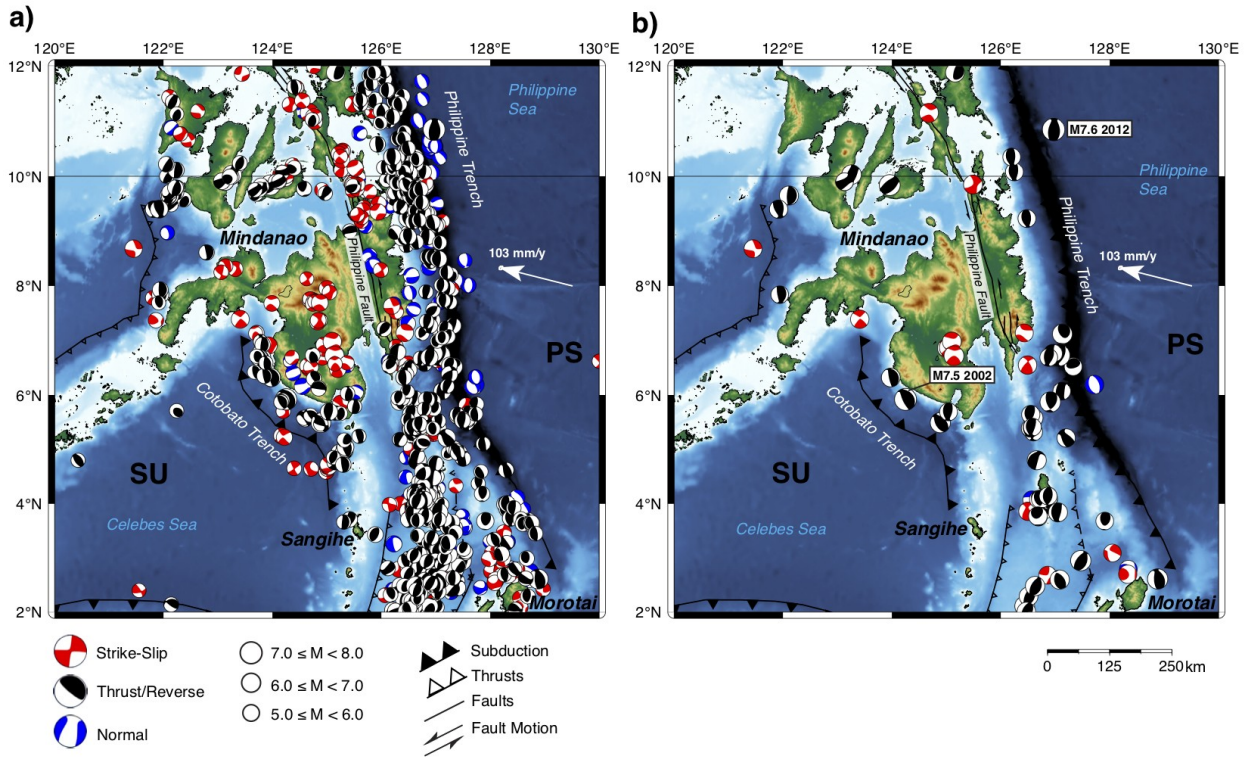

Figure 17. Shallow GCMT focal mechanisms ≤ 70 km depth for the southern Philippines and Celebes Sea region between January 1, 2000 and July 28, 2020 for events (a) ≥ **M** 5.0 and (b) ≥ **M** 6.0. Events are colored by mechanism and scaled by magnitude. Thrusting is active within the Philippine trench but events are < **M** 6.0. Active megathrusting is prevalent at the Cotobato trench. Strike-slip motion is located primarily along the Philippine fault. Outer-rise normal faulting is similar to Java, with a single reverse event in 2012 suggesting a locked megathrust (Christensen and Ruff, 1988; Ye et al., 2012). Notable events labeled in panel (b) are presented in Table 3. Faults are obtained from Moore and Silver (1983), Widiwijayanti et al. (2004), Besana and Ando (2005), Tsutsumi and Perez (2013), and Hall (2018). White arrows represent plate velocities with respect to the Sunda plate from the MORVEL velocity model (DeMets et al., 2010). SU = Sunda plate, and PS = Philippine Sea plate.

Megathrust activity may still occur in regions where collision and accretion have recently overprinted subduction (Figures 18 and 19). Bird (2003) indicated that the Molucca Sea Collision Zone is likely capable of megathrusting if an interface with the subducted Molucca Sea plate is present beneath the colliding Sangihe and Halmahera arcs (Figure 18). Some focal mechanisms ≥ **M** 5.0 suggest thrust faults that dip to the west near Sulawesi and to the east near

841 Halmahera, consistent with the orientations of the Molucca Sea plate (Figures 6 and 18a).
842 However it is not clear whether these events may represent interplate slip. Similarly,
843 megathrusting may be possible within the Timor and Seram troughs (Figure 19. Liu and Harris,
844 2014). Despite often being interpreted as foreland basins that formed during collision rather than
845 as active subduction zones (Audley-Charles, 2011; Patria and Hall, 2017), some authors have
846 argued that the Seram trough in particular is still an active subduction zone (Bird, 2003;
847 Hinschberger et al., 2005). Focal mechanisms ≥ **M** 5.0 are supportive of north-dipping thrusts
848 inboard of the Timor trough and south-dipping thrusts inboard of the Seram trough, consistent
849 with the orientation of subduction at these locations (Figure 19a; Spakman and Hall, 2010;
850 Widiyantoro et al., 2011b; Hall and Spakman, 2015). However, it is not clear whether these
851 events are representative of ruptures at a plate interface, deformation within the overlying
852 continental crust, or within underlying continental crust due to continental subduction
853 (Hinschberger et al., 2005; Tate et al., 2015). Using historical records, Liu and Harris (2014)
854 modeled a megathrust event that likely occurred within the Seram trough in 1629 that resulted in
855 a destructive tsunami. This result indicates that megathrust events are possible beneath Seram,
856 but are rare.

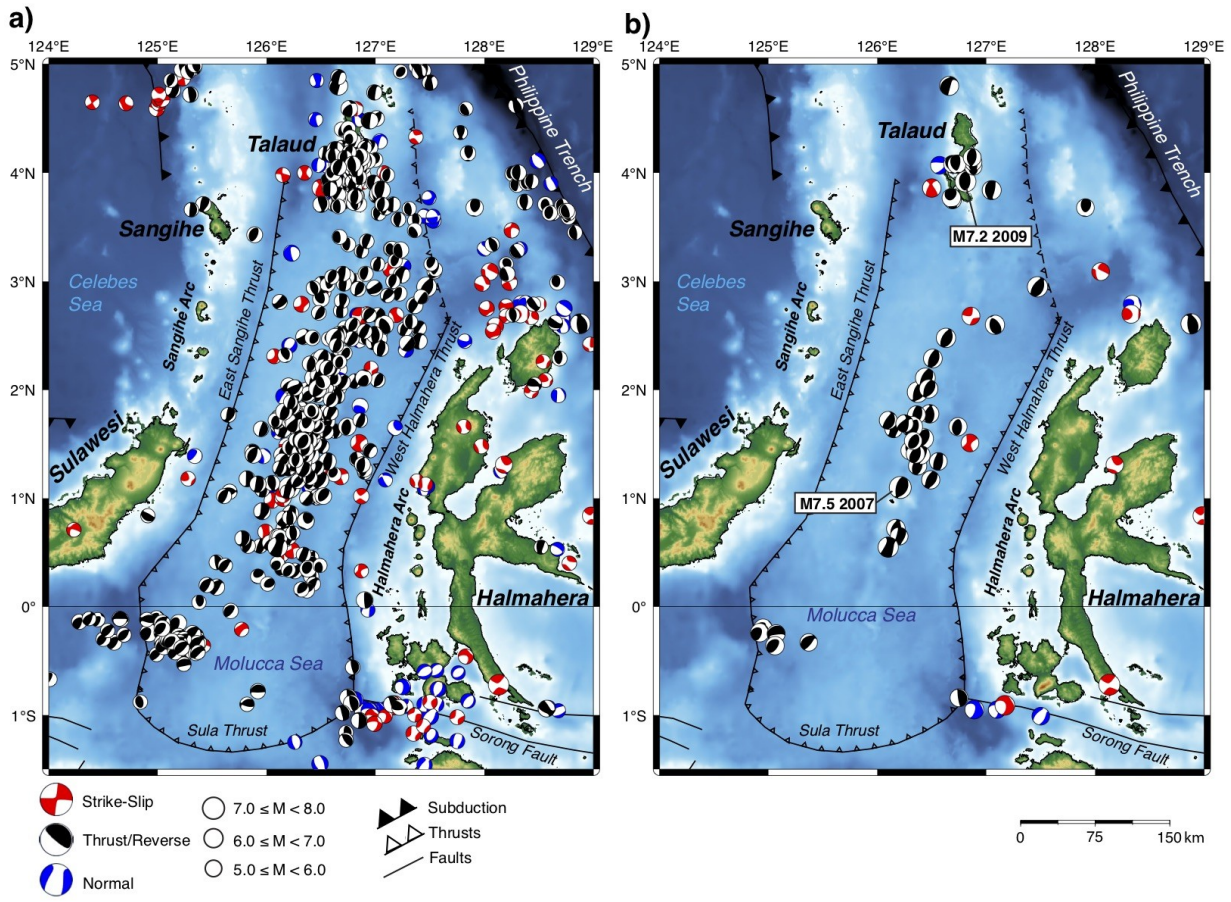

Figure 18. Shallow GCMT focal mechanisms ≤ 70 km depth for the Molucca Sea Collision Zone between January 1, 2000 and July 28, 2020 for events (a) ≥ **M** 5.0 and (b) ≥ **M** 6.0. Events are colored by mechanism and scaled by magnitude. Thrust and reverse faulting is concentrated between the East Sangihe and West Halmahera thrusts, reflecting deformation from ongoing collision between the Sangihe and Halmahera arcs. Notable events labeled in panel (b) are presented in Table 3. Faults are obtained from Moore and Silver (1983), Widiwijayanti et al. (2004), Tsutsumi and Perez (2013), Saputra et al. (2014), Watkinson et al. (2011), Watkinson and Hall (2017), and Hall (2018).

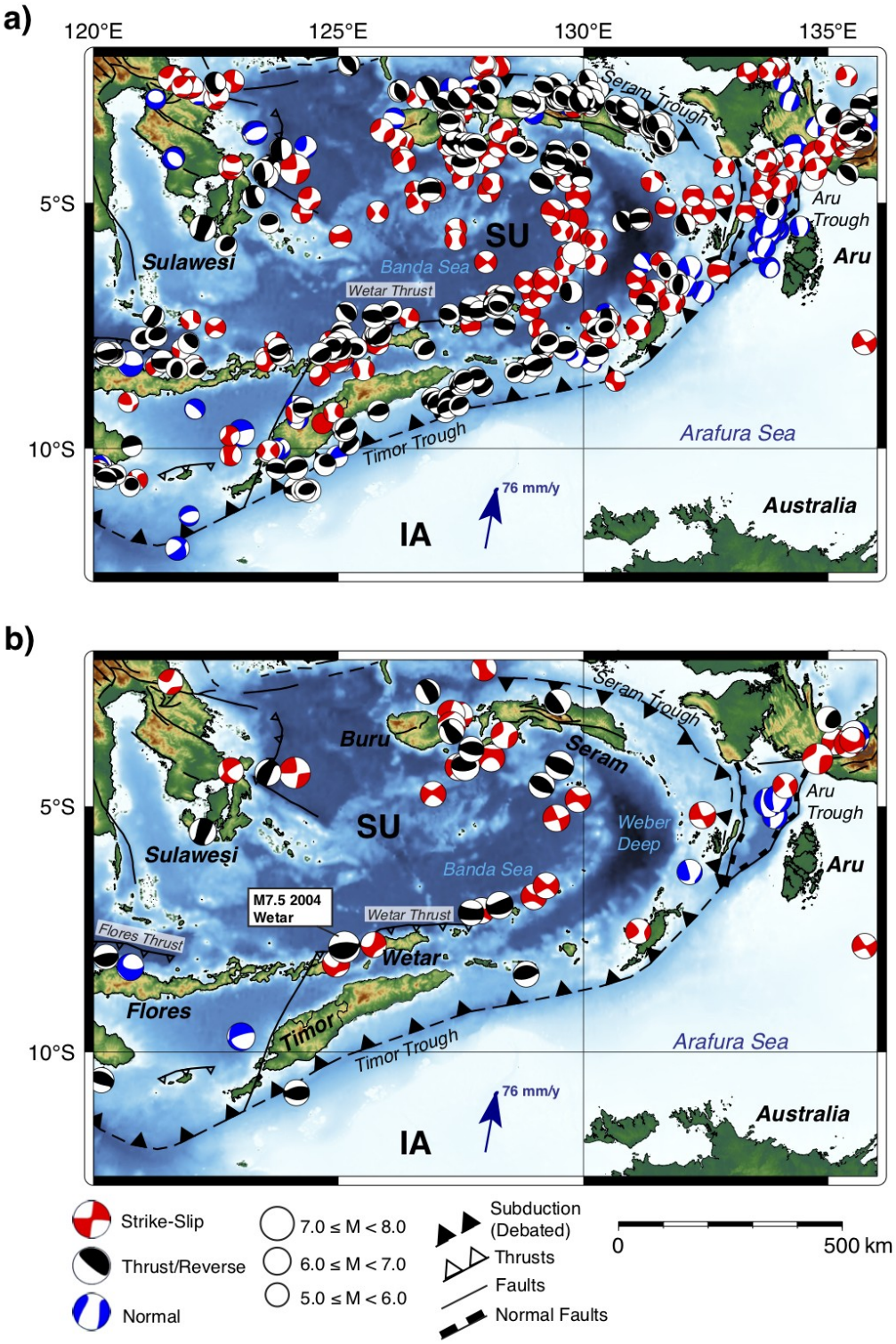

Figure 19. Shallow GCMT focal mechanisms ≤ 70 km depth for the Banda Sea between January 1, 2000 and July 28, 2020 for events (a) ≥ **M** 5.0 and (b) ≥ **M** 6.0. Events are colored by mechanism and scaled by magnitude. Thrusting is active inboard of the Timor and Seram

870 troughs and along the Wetar and Flores back-arc thrusts. The back-arc thrusts may represent
871 subduction polarity reversal (Silver et al., 1983b). Strike-slip and reverse events throughout the
872 Banda Sea indicate complex transpressive motion. Notable events labeled in panel (b) are
873 presented in Table 3. Faults are obtained from Silver et al. (1983b), Roosmawati and Harris
874 (2009), Watkinson et al. (2011), Saputra et al. (2014), Cipta et al. (2016), Koulali et al. (2016),
875 Adhitama et al. (2017), Patria and Hall (2017), Watkinson and Hall (2017), Hall (2018), Nugraha
876 and Hall (2018), and Valkaniotis et al. (2018). Blue arrows represent plate velocities with respect
877 to the Sunda plate obtained from the MORVEL velocity model (DeMets et al., 2010). SU =
878 Sunda plate, and IA = Indo-Australian plate.

879 4.4.2 Crustal Seismicity

880 Deformation of the crust is an important source of shallow seismicity in Indonesia,
881 though the locations of crustal faults remain a subject of debate. Efforts to accurately locate
882 faults throughout Indonesia have been reported in recent years (Sieh and Natawidjaja, 2000;
883 Saputra et al., 2014; Cipta et al., 2016; Omang et al., 2016; Patria and Hall, 2017; Watkinson and
884 Hall, 2017; Supendi et al., 2018; Irsyam et al., 2020). The thickness of the continental crust of
885 the Sunda plate is highly variable, ranging between 27-42 km (Wölbern and Rümpker, 2016; Ali
886 and Suardi, 2018; Suhardja et al., 2020). We divide crustal seismicity into three primary faulting
887 types, being (1) thrust, (2) strike-slip, and (3) normal.

888 4.4.2.1 Thrust Faulting

889 Thrust faulting is commonly observed inboard of subduction zones and within regions of
890 active collision. In the Molucca Sea Collision Zone (Figure 18), prominent thrust faults on the
891 margins of the colliding Sangihe and Halmahera volcanic arcs accommodate the majority of E-
892 W convergence (~80 mm/y) between the Sunda and Philippine Sea plates (Figures 17 and 18;
893 Rangin et al., 1999; Bock et al., 2003). The primary faults are the West Halmahera thrust on the
894 western margin of the Halmahera arc, and the East Sangihe thrust on the eastern margin of the
895 Sangihe arc, which dip toward each other toward the center of the collision zone (Figure 18;
896 Moore and Silver, 1983). Abundant reverse and thrust faulting mechanisms ≥ **M** 5.0 with NE-
897 SW strikes located between the thrusts reflect deformation between the colliding arcs (Figure
898 18a). Five events ≥ **M** 7.0 have occurred in the region since January 2000, the largest being a $\mathbf{M}_w$

899 7.5 rupture in 2007 (Figure 18b; Table 3). Some events have caused damage to Sulawesi and
900 Talaud islands, and particular events such as the 2019 $\mathbf{M}_w$ 7.1 Molucca Sea earthquake generated
901 small tsunamis, indicating that frequent thrust activity in the Molucca Sea region creates notable
902 seismic hazard for nearby islands including Sulawesi, Talaud, Halmahera, and Sangihe (Table 3;
903 U.S. Geological Survey, 2020).

904 In the Banda and Flores seas, the Flores and Wetar back-arc thrusts form an
905 approximately 800 km-long south-dipping thrust system that traces offshore north of the islands
906 of Lombok, Sumbawa, Flores, and Wetar (Figures 14 and 19). Bock et al. (2003) indicate from
907 GPS measurements that the majority of convergence between the Indo-Australian and Sunda
908 plates at this location is accommodated by the thrusts (up to ~67 mm/y), representing the transfer
909 of convergence into the back-arc region and early subduction polarity reversal (Silver et al.,
910 1983b; Koulali et al., 2016). Focal mechanisms ≥ **M** 5.0 support south-dipping thrusts (Figure
911 14a and 19a). Back-arc thrusting activity decreases west of the Flores thrust toward the Kendeng
912 thrust in Java, where two events ≥ **M** 5.0 support a south-dipping thrust (Figure 14a). The
913 majority of the Kendeng thrust appears to be seismically inactive due to a lack of events near the
914 fault (Figures 14a-b), however, Koulali et al. (2016) indicate from GPS data that the fault is
915 active and a likely extension of the Flores thrust. Both the Flores and Wetar thrusts have
916 generated several notable and damaging events recently, such as the 2018 Lombok Sequence
917 which produced two $\mathbf{M}_w$ 6.9 events north of Lombok (Figure 14b; Table 3; Yang et al., 2020),
918 and a $\mathbf{M}_w$ 7.5 event near Wetar in 2004 (Figure 19b; Table 3; Hayes et al., 2017; U.S. Geological
919 Survey, 2020). As much of the active thrusting occurs offshore, there is great risk for tsunamis.
920 For example, the 1992 $\mathbf{M}_w$ 7.9 Flores Earthquake generated a tsunami with wave heights up to 25
921 m (Yeh et al., 1993; Yang et al., 2020).

922 Abundant focal mechanisms ≥ **M** 5.0 also indicate activity on SW-dipping thrust faults
923 on the north coast of Seram, with the largest event being a $\mathbf{M}_w$ 6.3 in 2006 (Figure 16a;
924 Watkinson and Hall, 2017; U.S. Geological Survey, 2020). Other thrusts such as Sulawesi's
925 Batui, Tolo,and Makassar thrusts exhibit little to no seismicity ≥ **M** 5.0 (Figure 15; Watkinson
926 and Hall, 2017). The Makassar thrust however has been designated a notable seismic hazard
927 based on earthquake hazard modeling (Cipta et al., 2016; Irsyam et al., 2020).

928 4.4.2.2 Strike-Slip Faulting

Oblique convergence in Indonesia produces a considerable amount of lateral motion accommodated by strike-slip fault zones. In western Indonesia, the ~1900 km-long, segmented dextral Sumatran fault traces the length of Sumatra and partitions oblique subduction at the Sunda-Java trench (Figure 13a; Sieh and Natawidjaja, 2000; McCaffrey, 2009). Partitioning of dextral slip along this major plate boundary fault has been proposed to form a "sliver plate" in the forearc between the fault and the megathrust that behaves separately from the rest of the Sunda plate (McCaffrey, 2009; Bradley et al., 2017). The nature of the sliver plate is debated, with some authors proposing that increasing slip rates along the Sumatran fault moving north inferred by GPS imply the forearc is stretching (Bock et al., 2003; McCaffrey, 2009). More recent modeling by Bradley et al. (2017) however suggests that the forearc is rigid, and the Sumatran fault accommodates a constant slip rate ~15-16 mm/y. The Sumatran fault exhibits notable seismic activity, with five events between **M** 6.0 – 7.0 confirmed to have occurred on the fault in the past two decades, the largest being a $\mathbf{M}_w$ 6.6 event in 2009 (Figure 13b; Salman et al., 2020; U.S. Geological Survey, 2020). Some of these events were damaging (Salman et al., 2020). The fault zone is estimated to be capable of ~**M** 7.5-7.7 ruptures (McCloskey et al., 2005), with a 1995 **M** 7.0 rupture in southern Sumatra being the most recent major earthquake (Sieh and Natawidjaja, 2000; McCaffrey, 2009; Omang et al., 2016). Seismicity may be induced on the Sumatran fault directly by great megathrust events generated at the Sunda megathrust (McCloskey et al., 2005), and related faults that lie outside of the Sumatran fault zone pose additional hazards, such as the fault responsible for the damaging 2016 $\mathbf{M}_w$ 6.6 Aceh earthquake (Figure 13b; Salman et al., 2020)

Offshore of Sumatra, a series of N-S trending strike-slip faults within the oceanic crust of the Indo-Australian plate further add to seismicity (Figure 13a). Abundant strike-slip mechanisms ≥ **M** 5.0 west of Sumatra between 0-5˚N support activity on these faults (Figure 13a), which likely represent reactivated fracture systems formed during now extinct seafloor spreading in the Wharton Basin (Indian Ocean; Satriano et al., 2012). Activity on these faults may be indicative of diffuse deformation between the Indian and Australian plates, referred to as a single plate (Indo-Australian plate) throughout this paper (Bradley et al., 2017). While reasons for this deformation are debated, Bradley et al. (2017) indicate that for their rigid Sumatran forearc model to be plausible, the majority of deformation must be accommodated within the oceanic crust of the Indo-Australian plate. These remarkable faults generated the largest strike-

slip events ever recorded in 2012, a $\mathbf{M}_w$ 8.6 and a $\mathbf{M}_w$ 8.2 (Figure 13b; Table 3), which were likely induced by Coulomb stress changes following the December 2004 $\mathbf{M}_w$ 9.1 Sumatra-Andaman and March 2005 $\mathbf{M}_w$ 8.6 Nias events (Delescluse et al., 2012).

Eastern Indonesia is decidedly more complex, with several strike-slip fault zones accommodating E-W sinistral shear between the obliquely converging Pacific (Philippine Sea and Caroline plates) and Indo-Australian plates (Figure 16). The Sorong fault for example trends E-W from the Bird's Head to near eastern Sulawesi (Figures 1 and 16), splitting into several "horsetail" splays west of the Bird's Head (Figures 1 and 16; Watkinson et al., 2011; Saputra et al., 2014; Watkinson and Hall, 2017). A lack of strike-slip focal mechanisms ≥ **M** 5.0 near the Sorong fault at the Bird's Head suggests the fault is not very seismically active at this location (Figure 16a; Watkinson and Hall, 2017). Increased strike-slip activity ≥ **M** 5.0 is evident to the west near Halmahera island (Figure 16a), where the fault on average is estimated to accommodate ~19 mm/y of slip (Bock et al., 2003; Watkinson and Hall, 2017). The western splays of the Sorong fault have generated notable events, such as 2019 $\mathbf{M}_w$ 7.2 earthquake south of Halmahera (Figure 16b; Table 3; U.S. Geological Survey, 2020).

Strike-slip mechanisms ≥ **M** 5.0 supportive of E-W sinistral shear are also evident east of the Bird's Head, where the Sorong fault connects to the Yapen fault (Figure 16; Hinschberger et al., 2005; Patria and Hall, 2017; Watkinson and Hall, 2017). The Yapen fault is estimated to accommodate ~46 mm/y of slip, with the majority of seismicity ≥ **M** 6.0 clustered near its connection with the Sorong fault where a destructive $\mathbf{M}_w$ 7.6 earthquake occurred in 2002 (Figure 16b; Table 3; Hayes et al., 2017). Strike-slip events ≥ **M** 5.0 also support E-W sinistral motion south of the Yapen fault to the E-W trending Terera-Aiduna and NE-SW trending Lowland faults (Figure 16; Watkinson and Hall, 2017). This supports the hypothesis that sinistral shear on a broad scale is transferred south from the Yapen fault to the Terera-Aiduna fault, effectively bypassing the Sorong fault at the Bird's Head (Bock et al., 2003; Hinschberger et al., 2005; Watkinson and Hall, 2017). The Terera-Aiduna and Lowland faults have produced several events ≥ **M** 6.0 recently, the largest being the 2004 $\mathbf{M}_w$ 7.3 Nabire earthquake (Figure 16b; Table 3; Hayes et al., 2017). Strike-slip seismicity extends westward beyond the Terera-Aiduna fault and into the Banda Sea, where sinsitral shear is likely transferred to the western Sorong fault via transpressive faults across Seram (Patria and Hall, 2017; Watkinson and Hall, 2017). This proposed transfer of sinistral shear from the Terera-Aiduna fault to faults on Seram is not

991 distinguishable from seismicity alone, and Watkinson and Hall (2017) suggest any connection
992 may be aseismic or there is no structural connection at all.
993 Notable strike-slip faults on Seram include the sinistral Kawa and Bobol faults (Figure
994 16; Patria and Hall, 2017; Watkinson and Hall, 2017). Few strike-slip focal mechanisms ≥ **M** 5.0
995 are evident along these faults, though geomorphic expressions interpreted by Watkinson and Hall
996 (2017) indicate the Kawa fault is capable of ground-rupturing events, as are other faults on the
997 island, such as the recently reactivated fault responsible for the destructive 2019 $\mathbf{M}_w$ 6.5 Ambon
998 earthquake (Figure 16b; Table 3; Sahara et al., 2021). Mixed strike-slip and reverse mechanisms
999 ≥ **M** 5.0 between Seram island and the western Sorong fault suggest the transfer of sinstral shear
1000 between them is very complex. Additionally, strike-slip mechanisms ≥ **M** 5.0 in the Banda Sea
1001 between Seram and Wetar to the south suggest that lateral motion may be partitioned by faults
1002 throughout the interior of the Banda Sea, possibly along remnants of older seafloor spreading,
1003 though this is speculative (Figures 16 and 19; Bock et al., 2003; Hinschberger et al, 2005; Seton
1004 et al., 2020).
1005 Farther west on the island of Sulawesi, sinistral-shear is accommodated primarily by the
1006 Montano and Palu-Koro faults (Figure 15; Silver et al, 1983a; Socquet et al., 2006; Watkinson
1007 and Hall, 2017). The Montano fault is a highly segmented SE-NW trending fault system that
1008 extends offshore to the east toward the Tolo thrust, and inland to connect with the southern
1009 terminus of the Palu-Koro fault though the nature of this connection is not well understood
1010 (Figure 15; Silver et al, 1983a; Watkinson and Hall, 2017). Strike-slip mechanisms ≥ **M** 5.0
1011 supportive of E-W sinistral shear are clustered along the eastern Montano fault with the largest
1012 event being a $\mathbf{M}_w$ 6.1 in 2011 (Figure 15; Watkinson and Hall, 2017). The western segments of
1013 the Montano fault do not exhibit any recent seismic activity ≥ **M** 5.0 (Figure 15). The ~220 km
1014 long Palu-Koro fault trends NW from near the Bone Bay and extends offshore to the western
1015 extent of the North Sulawesi trench (Figure 15; Silver et al., 1983a; Watkinson and Hall, 2017;
1016 Hall, 2018; Patria and Putra, 2020). Strike-slip mechanisms near the fault support NW-SE
1017 sinistral shear with slip rates estimated from GPS at ~ 38 mm/y (Figure 15; Bock et al., 2003;
1018 Watkinson and Hall, 2017). The Palu-Koro and Montano faults have been recognized as serious
1019 seismic hazards (Cipta et al., 2016; Watkinson and Hall, 2017; Irsyam et al., 2020). The Palu-
1020 Koro fault in particular has produced several events ≥ **M** 6.0 in the past two decades, the largest
1021 being the September 2018 $\mathbf{M}_w$ 7.5 Palu earthquake, which caused an uncharacteristically large

tsunami and widespread liquefaction that devastated Palu (Figure 15; Table 3; Socquet et al., 2019).

Other strike-slip faults on Sulawesi have exhibited little to no seismic activity recently, though may be tectonically active and sources of future seismicity based on earthquake hazard modeling and GPS studies (Figure 15; Socquet et al., 2006; Cipta et al., 2016; Watkinson and Hall, 2017; Irsyam et al., 2020). The onshore segment of the Lawanopo fault (Figure 15) for example, which runs roughly parallel and south of the Montano fault has been previously classified as a serious earthquake hazard (Cipta et al., 2016; Watkinson and Hall, 2017; Irsyam et al., 2020). The offshore segment of the fault or a related fault likely produced the 2001 $\mathbf{M}_w$ 7.5 Banda Sea earthquake (Figure 15; Table 3; Hayes et al., 2017; Watkinson and Hall, 2017). The Walanae and Gorontalo faults (Figure 15) have also been identified as potential sources of seismic hazard (Cipta et al., 2016; Irsyam et al., 2020). Though they exhibit little to no seismicity, there is indication that the faults are currently locked, based on low slip rates derived primarily from GPS data (Socquet et al., 2006; Cipta et al., 2016; Watkinson and Hall, 2017). In eastern Sulawesi, the E-W trending dextral Balantak fault exhibits little to no apparent seismicity supporting dextral shear from available focal mechanisms, but has been suggested to be tectonically active (Figure 15; Watkinson and Hall, 2017). The majority of strike-slip activity in eastern Sulawesi lies on a series of NE-SW trending faults that cross the Banggai islands (Figure 15; Watkinson et al., 2011; Watkinson and Hall, 2017). These complex dextral-transpressive faults pose serious seismic hazards, and produced the destructive $\mathbf{M}_w$ 7.6 Banggai islands earthquake and tsunami in May 2000 (Hayes et al., 2017; Watkinson and Hall, 2017).

4.4.2.3 Normal Faulting

Crustal normal faulting is abundant in eastern Indonesia, commonly intermixed with reverse and strike-slip faulting in transpressive regions such as the Banda Sea, Sulawesi, and West Papua (Figures 15, 16, and 19). Prominent zones of normal faulting include the Aru trough (Figure 16) and the Gulf of Tomini (Figure 15), with extension attributed to slab-rollback of the Banda and Celebes slabs respectfully (Spakman and Hall, 2010; Hall and Spakman, 2015; Adhitama et al., 2017). Normal faulting mechanisms ≥ **M** 5.0 in the Aru trough support N-S trending faults and E-W extension (Figure 16a; Bird, 2003; Adhitama et al., 2017), where the Banda Sea moves approximately ~15-18 mm/y westward away from the Indo-Australian plate

(Bock et al., 2003; Hayes et al., 2017). The largest recent event in the Aru trough was a $\mathbf{M}_w$ 7.0 in 2010 (Table 3; Hayes et al., 2017). In addition to the Aru trough, slab rollback in this region likely formed the Weber Deep, where a low angle normal fault termed the Banda detachment has never generated any recorded seismicity but may have caused the 1852 Banda Tsunami (Cummins et al., 2020). Similarly to the Aru trough, normal faulting events ≥ **M** 5.0 in Sulawesi's Gulf of Tomini (Figure 15) are supportive of NW-SE-striking normal faults and NE-SW extension that extends into the Togean islands consistent with rollback of the Celebes slab (Hall and Spakman, 2015; Watkinson and Hall, 2017; Hall, 2018).

Normal faulting is also common within the outer-rise regions of subducting plates, forming narrow trench-parallel seismic zones within the oceanic crust. Several extensional events ≥ **M** 5.0 south of the Sunda-Java trench near Java (Figure 14a), and a similar zone east of the Philippine trench (Figure 17a) support down-dip extension (slab-pull) associated with outer-rise normal faulting (Christensen and Ruff, 1988). Outer-rise faulting can provide insight into the state of stress on the megathrust. Abundant outer-rise normal faulting combined with few megathrust events suggests weak coupling on the megathrust, whereas reverse faulting in the outer-rise suggests strong coupling (Christensen and Ruff, 1988). The lack of large megathrust events and abundant outer-rise normal faulting from Java to Sumba suggests weak coupling on the eastern Sunda megathrust, supporting prior interpretations (Irsyam et al., 2020). The Philippine trench in contrast may exhibit strong coupling east of Mindanao due to infrequent thrust faulting in the outer-rise (Figure 17; Ye et al., 2012). Though rare, outer-rise normal faults can generate events ≥ **M** 7.0. The largest normal faulting event ever recorded occurred within the outer-rise south of Sumba in 1977, producing a massive $\mathbf{M}_w$ 8.3 earthquake and an eight-meter tsunami that devastated Sumba and Sumbawa islands (Lynnes and Lay, 1988; Gusman et al., 2009). The possibilities of damaging singular events in the outer rise, or events preceding or following large megathrust events further compounds elevated seismic hazards at these subduction zones.

4.4.3 Shallow Intraslab Seismicity

Shallow intraslab events can occur by the same diverse mechanisms discussed in Section 4.3.7, but are constrained to between ~20-60 km depth and often occur directly below the active megathrust interface (Seno and Yoshida, 2003; Wiseman et al., 2012). Individual events are

capable of reaching magnitudes ≥ **M** 7.0, and pose notable seismic hazard. The June 2000 $\mathbf{M}_w$ 7.9 Enganno event for example occurred as an oblique mechanism ~33-50 km depth beneath the southern Sumatran forearc and caused significant damage and fatalities to local communities (Figure 13b; Table 3; Abercrombie et al., 2003; Wiseman et al., 2012; U.S. Geological Survey, 2020). Events can also compound seismic hazards already inherent with active megathrusting, capable of both inducing and being induced by megathrust ruptures (Wiseman et al., 2012).

5 Conclusions

This synthesis of the seismicity of Indonesia permits the following observations and conclusions.

(1) The Indonesian region has a very high level of seismic activity, exhibiting an average of about 320 ≥ **M** 5.0 earthquakes each year with events ≥ **M** 7.0 not uncommon, including the occurrence of four great (≥ **M** 8.0) earthquakes since January 2000. The sources of seismicity are diverse, and include active megathrusts, crustal faults, and normal and reverse intraslab mechanisms. The majority of seismicity (77%) is shallow (≤ 70 km) and concentrated at or near plate boundaries and major faults. Abundant intermediate and deep seismicity (≥ 70 km depth) accounts for ~23% of all seismicity and traces the Wadati-Benioff zones of subducting slabs with orientations generally consistent with recent tomography models and Indonesian tectonics.

(2) Intermediate and deep seismicity distributions and mechanisms vary greatly by location and depth. Regionally, seismicity rates decrease exponentially with depth and increase within the MTZ, consistent with global seismicity-depth distributions. Viscous resistance from phase changes at the 410, 520, and 660 km phase boundaries likely contributes to elevated seismicity rates within the MTZ, with the highest rates in the Celebes and Banda Sea regions of eastern Indonesia. The frequency of deep events decreases westward across Java toward Sumatra, likely due to increasing oblique convergence, decreasing lithospheric age, and increasing mantle temperatures. Similarly, lithospheric age and oblique convergence likely contribute to poorly developed Wadati-Benioff zones in the Makokwari trough and western New Guinea trench. Seismic gaps in Wadati-Benioff zones are common, with some inferred to be related to slab tearing (e.g. east Java and Timor), while others are not clearly understood (e.g. Sangihe and Philippine Sea slabs). Intraslab source mechanisms are diverse, with normal faulting commonly observed for deep events, and oblique-reverse mechanisms common at intermediate

depths. Individual events are capable of reaching magnitudes ≥ **M** 7.0 and can pose notable seismic hazards such as the 2009 $\mathbf{M}_w$ 7.6 Padang earthquake.

(3) Shallow seismicity is diverse but is consistent with recent tectonic models for the location of crustal faults. The abundance and high magnitudes of shallow earthquakes also highlights the locations and sources of significant seismic hazards throughout the region. Shallow events pose greater seismic hazard due to hypocenters residing closer to the surface than intermediate and deep events. Megathrusting is a primary source of shallow seismicity, and a prevalent source of seismic and tsunami hazard. Crustal faulting occurs primarily on major thrust, strike-slip, and normal fault zones, with individual events more than capable of reaching ≥ **M** 7.0 and even great magnitudes. Regions with elevated seismic activity such as Sumatra, Sulawesi, the Banda Sea, and the Molucca Sea Collision Zone are clearly prone to prevalent seismic hazards, which beyond ground shaking may include liquefaction, landslides, and tsunamis. However, it is important to note that even less obvious regions with relatively subdued seismic activity, such as Java or the western New Guinea trench still pose notable seismic hazards (e.g. $\mathbf{M}_w$ 7.7 Java 2006). Therefore, nearly all regions of Indonesia should be quantitatively assessed for the seismic and tsunami hazard.

5.1 Further Study

While this study provides a comprehensive overview of the current knowledge of Indonesian seismotectonics, there are several regions where further study is needed to provide a more complete analysis. For example, in West Papua, the nature of subduction at the Manokwari trough and western New Guinea trench is not well documented and would benefit from further study. In addition, the origin of seismic gaps, such as the gap in the Sangihe slab beneath Mindanao or the aseismicity of the Philippine Sea slab require further study. Addressing these regions would improve the assessment of Indonesian seismotectonics.

6 Acknowledgements and Data Availability

Support is gratefully acknowledged from the USGS Earthquake Hazards Program and the Bureau of Humanitarian Affairs of the U.S. Agency for International Development (USAID). Funding for this research is provided through the USAID Grant # USGS GR12 2020. This study greatly benefitted from reviews of an earlier draft by M. Barazangi, T. Lay, K. Haynie, and P.

McCrory. The authors declare no conflicts of interest. Data resources are from the National Earthquake Information center (NEIC, USGS) and the Global Centroid Moment Tensor (GCMT) project, available at https://www.usgs.gov/natural-hazards/earthquake-hazards/earthquakes, and https://www.globalcmt.org/ respectively. Data used to compare USGS locations for location uncertainty are from the International Seismological Center (ISC) Bulletin, available at http://www.isc.ac.uk/iscbulletin/search/catalogue/. The MORVEL plate velocity online calculator (DeMets et al., 2010) is available at http://geoscience.wisc.edu/~chuck/MORVEL/citation.html. Grid files for plotting seafloor ages created by Seton et al. (2020) are available at https://www.earthbyte.org/category/resources/data-models/seafloor-age/. USGS Slab 2.0 (Hayes, 2018) is available at https://www.sciencebase.gov/catalog/item/5aa1b00ee4b0b1c392e86467. The latest versions of Generic Mapping Tools software (Wessel et al., 2019) and associated remote datasets are available for download at https://www.generic-mapping-tools.org/download/.

7 References

Abercrombie, R. E., Antolik, M., & Ekström, G. (2003). The June 2000 M_w 7.9 earthquakes south of Sumatra: Deformation in the India-Australia plate. *Journal of Geophysical Research: Solid Earth, 108*(B1), 2018. https://doi.org/10.1029/2001JB000674

Adhitama, R., Hall, R., & White, L. T. (2017). Extension in the Kumawa block, West Papua, Indonesia. In *Indonesian Petroleum Association, Proceedings 41st Annual Convention* (pp. IPA17-125-G 1-17). Indonesian Petroleum Association. https://doi.org/10.29118/IPA.50.17.125.G

Ali, Y. H., & Suardi, I. (2018). Crustal thickness beneath Jailolo region constructed from P wave receiver function. *AIP Conference Proceedings, 1987*(1), 020038. https://doi.org/10.1063/1.5047323

Audley-Charles, M. G. (2011). Tectonic post-collision processes in Timor. In R. Hall, M. A. Cottam, & M. E. J. Wilson (Eds.), *The SE Asian Gateway: History and Tectonics of the Australia-Asia Collision, Geological Society, London, Special Publications* (Vol. 355, pp. 241–266). The Geological Society of London. https://doi.org/10.1144/SP355.12

1169 Baldwin, S. L., Fitzgerald, P. G., & Webb, L. E. (2012). Tectonics of the New Guinea region.
1170 *Annual Review of Earth and Planetary Sciences, 40,* 495-520.
1171 https://doi.org/10.1146/annurev-earth-040809-152540

1172 Baroux, E., Avouac, J.-P., Bellier, O., & Sébrier, M. (2002). Slip-partitioning and fore-arc
1173 deformation at the Sunda trench, Indonesia. *Terra Nova, 10*(3), 139-144.
1174 https://doi.org/10.1046/j.1365-3121.1998.00182.x

1175 Besana, G. M., & Ando, M. (2005). The central Philippine Fault Zone: location of great
1176 earthquakes, slow events, and creep activity. *Earth, Planets and Space, 57,* 987-994.
1177 https://doi.org/10.1186/BF03351877

1178 Bilek, S. L., & Lay, T. (2018). Subduction zone megathrust earthquakes. *Geosphere, 14*(4),
1179 1468-1500. https://doi.org/10.1130/GES01608.1.

1180 Billen, M. I. (2020). Deep slab seismicity limited by rate of deformation in the transition zone.
1181 *Science Advances, 6*(22)**,** eaaz7692. https://doi.org/10.1126/sciadv.aaz7692

1182 Bird, P. (2003). An updated digital model of plate boundaries. *Geochemistry, Geophysics,*
1183 *Geosystems, 4*(3), 1027. https://doi.org/10.1029/2001GC000252

1184 Bock, Y., Prawirodirdjo, L., Genrich, J. F., Stevens, C. W., McCaffrey, R., Subarya, C., et al.
1185 (2003). Crustal motion in Indonesia from Global Positioning System measurements.
1186 *Journal of Geophysical Research, 108*(B8), 2367. https://doi.org/10.1029/2001JB000324

1187 Bradley, K. E., Feng, L., Hill, E. M., Natawidjaja, D. H., & Sieh, K. (2017). Implications of the
1188 diffuse deformation of the Indian Ocean lithosphere for slip partitioning of oblique plate
1189 convergence in Sumatra. *Journal of Geophysical Research: Solid Earth, 122,* 572-591.
1190 https://doi.org/10.1002/ 2016JB013549

1191 Cao, A., & Gao, S. S. (2002). Temporal variation of seismic b-values beneath northeastern Japan
1192 island arc. *Geophysical Research Letters, 29*(9), 48-1-48-3.
1193 https://doi.org/10.1029/2001GL013775

1194 Cardwell, R. K., Isaacks, B. L., & Karig, D. E. (1980). The spatial distribution of earthquakes,

1195 focal mechanism solutions and subducted lithosphere in the Philippine and northeastern
1196 Indonesian islands. In D. E. Hayes (Ed.) *The Tectonic and Geologic Evolution of the*
1197 *Southeast Asian Seas and Islands, Geophysical Monograph Series* (Vol. 23, pp. 1-35).
1198 American Geophysical Union. https://doi.org/ 10.1029/GM023p0001

1199 Charlton, T. R. (2000). Tertiary evolution of the Eastern Indonesia Collision Complex. *Journal*
1200 *of Asian Earth Sciences*, *18*(5), 603-631. https://doi.org/10.1016/S1367-9120(99)00049-8

1201 Christensen, D. H., & Ruff, L. J. (1988). Seismic coupling and outer rise earthquakes. *Journal of*
1202 *Geophysical Research: Solid Earth, 93*(B11), 13421-13444.
1203 https://doi.org/10.1029/JB093iB11p13421

1204 Cipta, A., Robiana, R., Griffin, J. D., Horspool, N., Hidayati, S., & Cummins, P. (2016). A
1205 probabilistic seismic hazard assessment for Sulawesi, Indonesia. In P. R. Cummins, & I.
1206 Meilano (Eds.), *Geohazards in Indonesia: Earth Science for Disaster Risk Reduction,*
1207 *Geological Society, London, Special Publications* (Vol. 441, pp. 133-152). The
1208 Geological Society of London. https://doi.org/10.1144/SP441.6

1209 Cummins, P. R., Pranantyo, I. R., Pownall, J. M., Griffin, J. D., Meilano, I., & Zhao, S. (2020).
1210 Earthquakes and tsunamis caused by low-angle normal faulting in the Banda Sea,
1211 Indonesia. *Nature Geoscience, 13*, 312-318. https://doi.org/ 10.1038/s41561-020-0545-x

1212 Delescluse, M., Chamot-Rooke, N., Cattin, R., Fleitout, L., Trubienko, O., & Vigny, C. (2012).
1213 April 2012 intra-oceanic seismicity off Sumatra boosted by the Banda-Aceh megathrust.
1214 *Nature, 490*, 240-244. https://doi.org/10.1038/nature11520

1215 DeMets, C., Gordon, R. G., & Argus, D. F. (2010). Geologically current plate motions.
1216 *Geophysical Journal International, 181,* 1-80. https://doi.org/10.1111/j.1365-
1217 246X.2009.04491.x

1218 Dokht, R. M. H., Gu, Y. J., & Sacchi, M. D. (2018). Migration imaging of the Java subduction
1219 zones. *Journal of Geophysical Research: Solid Earth, 123*, 1540-1558.
1220 https://doi.org/10.1002/2017JB014524

1221 Duputel, Z., Rivera, L., Kanamori, H., & Hayes, G. (2012). W phase source inversion for
1222 moderate to large earthquakes (1990-2010). *Geophysical Journal International, 189*(2),
1223 1125-1147. https://doi.org/10.1111/j.1365-246X.2012.05419.x

1224 Dziewonski, A. M., Chou, T.-A., & Woodhouse, J. H. (1981). Determination of earthquake
1225 source parameters from waveform data for studies of global and regional seismicity.
1226 *Journal of Geophysical Research*, *86*(B4), 2825-2852.
1227 https://doi.org/10.1029/JB086iB04p02825

1228 Ekström, G. (2015). Global seismicity: Results from systematic waveform analyses, 1976-2012.
1229 In G. Schubert (Ed.), *Treatise on Geophysics, Second Edition* (Vol. 4, pp. 467-475).
1230 Elsevier. https://doi.org/10.1016/B978-0-444-53802-4.00085-3

1231 Ekström, G., Nettles, M., & Dziewoński, A. M. (2012). The global CMT project 2004-2010:
1232 centroid-moment tensors for 13,017 earthquakes. *Physics of the Earth and Planetary*
1233 *Interiors*, *200-201*, 1-9. https://doi.org/10.1016/j.pepi.2012.04.002

1234 Fan, J., & Zhao, D. (2018). Evolution of the southern segment of the Philippine Trench:
1235 Constraints from seismic tomography. *Geochemistry, Geophysics, Geosystems, 19,* 4612-
1236 4627. https://doi.org/10.1029/2018GC007685

1237 Frohlich, C. (1989). The nature of deep-focus earthquakes. *Annual Review of Earth and*
1238 *Planetary Sciences, 17*, 227-254. https://doi.org/10.1146/annurev.ea.17.050189.001303

1239 Frohlich, C. (2006). Deep earthquakes. Cambridge University Press, Cambridge (U.K.).
1240 https://doi.org/10.1017/CBO9781107297562

1241 Fujiwara, T., Tamaki, K., Fujimoto, H., Ishii, T., Seama, N., Toh, H., et al. (1995).
1242 Morphological studies of the Ayu trough, Philippine Sea - Caroline plate boundary.
1243 *Geophysical Research Letters, 22*(2), 109-112. https://doi.org/10.1029/94GL02719

1244 Global Volcanism Program (2013). Volcanoes of the world, v. 4.9.1. E. Venzke (Ed.).
1245 Smithsonian Institution. Downloaded 02 Nov 2020.
1246 https://doi.org/10.5479/si.GVP.VOTW4-2013

1247 Gómez, J. M., Madariaga, R., Walpersdorf, A., & Chalard, E. (2000). The 1996 earthquakes in
1248 Sulawesi, Indonesia. *Bulletin of the Seismological Society of America, 90*(3), 739-751.
1249 https://doi.org/10.1785/0119990055

1250 Gusman, A. R., Tanioka, Y., Matsumoto, H., & Iwasaki, S.-I. (2009). Analysis of the tsunami
1251 generated by the great 1977 Sumba earthquake that occurred in Indonesia. *Bulletin of the*
1252 *Seismological Society of America, 99*(4), 2169-2179. https://doi.org/10.1785/0120080324

1253 Hall, R. (1987). Plate boundary evolution in the Halmahera region, Indonesia. *Tectonophysics,*
1254 *144*(4), 337-352. https://doi.org/10.1016/0040-1951(87)90301-5

1255 Hall, R. (2012). Late Jurassic-Cenozoic reconstructions of the Indonesian region and the Indian
1256 Ocean. *Tectonophysics, 570-571*, 1-41. https://doi.org/10.1016/j.tecto.2012.04.021

1257 Hall, R. (2014). Indonesian tectonics: Subduction, extension, provenance and more. In
1258 *Proceedings, Indonesian Petroleum Association 38th Annual Convention* (Vol. 1, pp.
1259 IPA14-G-360 1-13). Indonesian Petroleum Association.

1260 Hall, R. (2018). The subduction initiation stage of the Wilson cycle. In R. W. Wilson, G. A.
1261 Houseman, K. J. W. McCaffrey, A. G., Doré, & S. J. H. Buiter (Eds.), *Fifty Years of the*
1262 *Wilson Cycle Concept in Plate Tectonics, Geological Society, London, Special*
1263 *Publications* (Vol. 470, pp. 415-437). The Geological Society of London. https://doi.org/
1264 10.1144/SP470.3

1265 Hall, R., Cloke, I. R., Nur'aini, S., Puspita, S. D., Calvert, S. J., & Elders, C. F. (2009). The north
1266 Makassar Straits: What lies beneath? *Petroleum Geoscience, 15*(2), 147-158.
1267 https://doi.org/10.1144/1354-079309-829

1268 Hall, R., & Spakman, W. (2015). Mantle structure and tectonic history of SE Asia.
1269 *Tectonophysics, 658*, 14-45. https://doi.org/10.1016/j.tecto.2015.07.003

1270 Hanifa, N. R., Sagiya, T., Fumiaki, K., Efendi, J., Abidin, H. Z., & Meilano, I. (2020). Interplate
1271 coupling model off the southwestern coast of Java, Indonesia, based on continuous GPS
1272 data in 2008-2010. *Earth and Planetary Science Letters, 401,* 159-171.
1273 https://doi.org/10.1016/j.epsl.2014.06.010

1274 Harris, R. (2011). The nature of the Banda arc-continent collision in the Timor region. In D.
1275 Brown & P. D. Ryan (Eds.), *Arc Continent Collision, Frontiers in Earth Sciences Series*
1276 (Vol. 4, pp. 163-211). Springer-Verlag Berlin Heidelberg. https://doi.org/10.1007/978-3-
1277 540-88558-0_7

1278 Hayes, G. (2018). Slab2 - A comprehensive subduction zone geometry model. *U.S. Geological*
1279 *Survey Data Release*. U.S. Geological Survey. https://doi.org/10.5066/F7PV6JNV

1280 Hayes, G. P., Meyers, E. K., Dewey, J. W., Briggs, R. W., Earle, P. S., Benz, H. M., et al.
1281 (2017). Tectonic summaries of magnitude 7 and greater earthquakes from 2000 to 2015.
1282 *U.S. Geological Survey Open-File Report* (2016-1192, pp. 1-148). Reston, VA: U.S.
1283 Geological Survey. https://doi.org/10.3133/ofr20161192

1284 Henry, C., & Das, S. (2002). The M_w 8.2, 17 February 1996 Biak, Indonesia, earthquake:
1285 Rupture history, aftershocks, and fault plane properties. *Journal of Geophysical*
1286 *Research, 107*(B11), 2312. https://doi.org/10.1029/2001JB000796

1287 Hinschberger, F., Malod, J.-A., Réhault, J.-P., Villeneuve, M., Royer, J.-Y., & Burhanuddin, S.
1288 (2005). Cenozoic geodynamic evolution of eastern Indonesia. *Tectonophysics, 404*(1-2),
1289 91-118. https://doi.org/10.1016/j.tecto.2005.05.005

1290 Houston, H. (2015). Deep earthquakes. In G. Schubert (Ed.), *Treatise on Geophysics (Second*
1291 *Edition)* (Vol. 4, pp. 329-354). Elsevier. https://doi.org/10.1016/B978-0-444-53802-
1292 4.00079-8

1293 Hughes, K. L. H., Masterlark, T., & Mooney, W. D. (2010). Poroelastic stress-triggering of the
1294 2005 M8.7 Nias earthquake by the 2004 M9.2 Sumatra–Andaman earthquake. *Earth and*
1295 *Planetary Science Letters, 293*(3-4)**,** 289-299. https://doi.org/10.1016/j.epsl.2010.02.043

1296 International Seismological Centre (2021). On-line Bulletin. https://doi.org/10.31905/D808B830.
1297 Accessed 2021-02-16.

1298 Irsyam, M., Cummins, P. R., Asrurifak, M., Faizal, L., Natawidjaja, D. H., Widiyantoro, S., et al.
1299 (2020). Development of the 2017 national seismic hazard maps of Indonesia. *Earthquake*

Spectra, 36(1), 1-25. https://doi.org/10.1177/8755293020951206

Jacob, J., Dyment, J., & Yatheesh, V. (2014). Revisiting the structure, age, and evolution of the Wharton Basin to better understand subduction under Indonesia. *Journal of Geophysical Research: Solid Earth, 119*(1), 169-190. https://doi.org/10.1002/2013JB010285

Kanamori, H. (1986). Rupture process of subduction-zone earthquakes. *Annual Review of Earth and Planetary Sciences, 14*, 293-322. https://doi.org/10.1146/annurev.ea.14.050186.001453

Kong, F., Gao, S. S., Liu, K. H., Ding, W., & Li, J. (2020). Slab dehydration and mantle upwelling in the vicinity of the Sumatra subduction zone: Evidence from receiver function imaging of mantle transition zone discontinuities. *Journal of Geophysical Research: Solid Earth, 125*(9), e2020JB019381. https://doi.org/10.1029/2020JB019381

Koulali, A., Susilo, S., McClusky, S., Meilano, I., Cummins, P., Tregoning, P., et al. (2016). Crustal strain partitioning and the associated earthquake hazard in the eastern Sunda-Banda Arc. *Geophysical Research Letters, 43*(5), 1943-1949. https://doi.org/10.1002/2016GL067941

Lallemand, S. E., Popoff, M., Cadet, J.-P., Bader, A.-G., Pubellier, M., Rangin, C., & Deffontaines, B. (1998). Genetic relations between the central and southern Philippine trench and the Sangihe trench. *Journal of Geophysical Research: Solid Earth, 103*(B1), 933-950. https://doi.org/10.1029/97JB02620

Lay, T., Kanamori, H., Ammon, C. J., Nettles, M., Ward, S. N., Aster, R. C., et al. (2005). The great Sumatra-Andaman earthquake of 26 December 2004. *Science, 308*(5725), 1127-1133. https://doi.org/10.1126/science.1112250

Liu, Z. Y.-C., & Harris, R. A. (2014). Discovery of possible mega-thrust earthquake along the Seram trough from records of 1629 tsunami in eastern Indonesian region. *Natural Hazards*, *72*, 1311-1328. https://doi.org/10.1007/s11069-013-0597-y

Lynnes, C. S., & Lay, T. (1988). Source process of the great 1977 Sumba earthquake. *Journal of Geophysical Research: Solid Earth, 93*(B11), 13407-13420.

https://doi.org/10.1029/JB093iB11p13407

McCaffrey, R. (2009). The tectonic framework of the Sumatran subduction zone. *Annual Review of Earth and Planetary Sciences, 37,* 345-366. https://doi.org/10.1146/annurev.earth.031208.100212

McCloskey, J., Nalbant, S. S., & Steacy, S. (2005). Earthquake risk from co-seismic stress: Last year's Indonesian earthquake has increased seismic hazard in the region. *Nature, 434*, 291. https://doi.org/10.1038/434291a

Mignan, A., & Woessner, J. (2012). Estimating the magnitude of completeness for earthquake catalogs. *Community Online Resource for Statistical Seismicity Analysis.* https://doi.org/10.5078/corssa-00180805

Milsom, J., Masson, D., Nichols, G., Sikumbang, N., Dwiyanto, B., Parson, L., & Kallagher, H. (1992). The Manokwari trough and the western end of the New Guinea trench. *Tectonics, 11*(1), 145-153. https://doi.org/10.1029/91TC01257

Moore, G. F., & Silver, E. A. (1983). Collision processes in the northern Molucca Sea. In D. E. Hayes (Ed.), *The Tectonic and Geologic Evolution of Southeast Asian Seas and Islands: Part 2, Geophysical Monograph Series* (Vol. 27, pp. 360-372). American Geophysical Union. https://doi.org/10.1029/GM027p0360

Newcomb, K. R., & McCann, W. R. (1987). Seismic history and seismotectonics of the Sunda arc. *Journal of Geophysical Research: Solid Earth, 92*(B1), 421-439. https://doi.org/10.1029/JB092iB01p00421

Nugraha, A. M. S., & Hall, R. (2018). Late Cenozoic paleogeography of Sulawesi, Indonesia. *Palaeogeography, Palaeoclimatology, Palaeoecology, 490,* 191-209. https://doi.org/10.1016/j.palaeo.2017.10.033

Okal, E. A. (1999). Historical seismicity and seismotectonic context of the great 1979 Yapen and 1996 Biak, Irian Jaya earthquakes. *Pure and Applied Geophysics*, *154*, 633-675. https://doi.org/10.1007/s000240050247

1353 Okal, E. A. (2012). The south of Java earthquake of 1921 September 11: A negative search for a
1354 large interplate thrust event at the Java trench. *Geophysical Journal International, 190*(3),
1355 1657-1672. https://doi.org/10.1111/j.1365-246X.2012.05570.x

1356 Omang, A., Cummins, P. R., Robinson, D., & Hidayati, S. (2016). Sensitivity analysis for
1357 probabilistic seismic hazard analysis (PSHA) in the Aceh fault segment, Indonesia. In P.
1358 R. Cummins, & I. Meilano (Eds.), *Geohazards in Indonesia: Earth Science for Disaster*
1359 *Risk Reduction, Geological Society, London, Special Publications* (Vol. 441, pp. 121-
1360 131). The Geological Society of London. https://doi.org/10.1144/SP441.5

1361 Patria, A., & Hall, R. (2017). The origin and significance of the Seram trough, Indonesia. In
1362 *Proceedings, Indonesian Petroleum Association 41st Annual Convention* (pp. IPA17-19-G
1363 1-19). Indonesian Petroleum Association. https://doi.org/10.29118/IPA.50.17-19-G

1364 Patria, A., & Putra, P. S. (2020). Development of the Palu–Koro fault in NW Palu Valley,
1365 Indonesia. *Geoscience Letters, 7*, 1. https://doi.org/10.1186/s40562-020-0150-2

1366 Polet, J., & Kanamori, H. (2000). Shallow subduction zone earthquakes and their tsunamigenic
1367 potential. *Geophysical Journal International, 142*(3), 684-702.
1368 https://doi.org/10.1046/j.1365-246x.2000.00205.x

1369 Rangin, C., Pichon, X. L., Mazzotti, S., Pubellier, M., Chamot-Rooke, N., Aurelio, M., et al.
1370 (1999). Plate convergence measured by GPS across the Sundaland/Philippine Sea plate
1371 deformed boundary: The Philippines and eastern Indonesia. *Geophysical Journal*
1372 *International, 139*(2), 296-316. https://doi.org/10.1046/j.1365-246x.1999.00969.x

1373 Romeo, I., & Álvarez-Gómez, J. A. (2018). Lithospheric folding by flexural slip in subduction
1374 zones as source for reverse fault intraslab earthquakes. *Nature: Scientific Reports, 8*,
1375 1367. https://doi.org/10.1038/s41598-018-19682-7

1376 Roosmawati, N., & Harris, R. (2009). Surface uplift history of the incipient Banda arc-continent
1377 collision: Geology and synorogenic foraminifera of Rote and Savu Islands, Indonesia.
1378 *Tectonophysics, 479*(1-2), 95-110. https://doi.org/10.1016/j.tecto.2009.04.009

1379 Sahara, D. P., Nugraha, A. D., Muhari, A., Rusdin, A. A., Rosalia, S., Priyono, A., et al. (2021).

1380 Source mechanism and triggered large aftershocks of the Mw 6.5 Ambon, Indonesia
1381 earthquake. *Tectonophysics,799,* 228709. https://doi.org/10.1016/j.tecto.2020.228709

1382 Saita, T., Suetsugu, D., Ohtaki, T., Takenaka, H., Kanjo, K., & Purwana, I. (2002). Transition
1383 zone thickness beneath Indonesia as inferred using the receiver function method for data
1384 from the JISNET regional broadband seismic network. *Geophysical Research Letters,*
1385 *29*(7), 1115. https://doi.org/10.1029/2001GL013629

1386 Salman, R., Lindsey, E. O., Feng, L., Bradley, K., Wei, S., Wang, T., et al. (2020). Structural
1387 controls on rupture extent of recent Sumatran fault zone earthquakes, Indonesia. *Journal*
1388 *of Geophysical Research: Solid Earth, 125,* e2019JB018101. https://doi.org/
1389 10.1029/2019JB018101

1390 Saputra, A., Hall, R., & White, L. T. (2014). Development of the Sorong fault zone north of
1391 Misool eastern Indonesia. In *Proceedings, Indonesian Petroleum Association 38th Annual*
1392 *Convention* (pp. IPA14-G-086 1-14). Indonesian Petroleum Association.
1393 https://doi.org/10.29118/IPA.0.14.G.086

1394 Satriano, C., Kiraly, E., Bernard, P., & Vilotte, J.-P. (2012). The 2012 Mw 8.6 Sumatra
1395 earthquake: Evidence of westward sequential seismic ruptures associated to the
1396 reactivation of a N-S ocean fabric. *Geophysical Research Letters, 39*(15), L15302.
1397 https://doi.org/10.1029/2012GL052387

1398 Seno, T., & Yoshida, M. (2003). Where and why do large shallow intraslab earthquakes occur?
1399 *Physics of the Earth and Planetary Interiors, 141*(3), 183-206.
1400 https://doi.org/10.1016/j.pepi.2003.11.002

1401 Seton, M., Müller, R. D., Zahirovic, S., Williams, S., Wright, N. M., Cannon, J., et al. (2020). A
1402 global data set of present-day oceanic crustal age and seafloor spreading parameters.
1403 *Geochemistry, Geophysics, Geosystems, 21*(10), e2020GC009214.
1404 https://doi.org/10.1029/2020GC009214

1405 Sieh, K., & Natawidjaja, D. (2000). Neotectonics of the Sumatran fault, Indonesia. *Journal of*
1406 *Geophysical Research: Solid Earth, 105*(B12), 28295–28326.

https://doi.org/10.1029/2000JB900120

Silver, E. A., & Moore, J. C. (1978). The Molucca Sea collision zone, Indonesia. *Journal of Geophysical Research: Solid Earth, 83*(B4), 1681-1691. https://doi.org/10.1029/JB083iB04p01681

Silver, E. A., McCaffrey, R., & Smith R. B. (1983a). Collision, rotation, and the initiation of subduction in the evolution of Sulawesi, Indonesia. *Journal of Geophysical Research: Solid Earth, 88*(B11), 9407-9418. https://doi.org/10.1029/JB088iB11p09407

Silver, E. A., Reed, D., McCaffrey, R., & Joyodiwiryo, Y. (1983b). Back arc thrusting in the eastern Sunda arc, Indonesia: A consequence of arc-continent collision. *Journal of Geophysical Research: Solid Earth, 88*(B9), 7429-7448. https://doi.org/10.1029/JB088iB09p07429

Socquet, A., Hollingsworth, J., Pathier, E., & Bouchon, M. (2019). Evidence of supershear during the 2018 magnitude 7.5 Palu earthquake from space geodesy. *Nature Geoscience, 12,* 192-199. https://doi.org/10.1038/s41561-018-0296-0

Socquet, A., Simons, W., Vigny, C., McCaffrey, R., Subarya, C., Sarsito, D., et al. (2006). Microblock rotations and fault coupling in SE Asia triple junction (Sulawesi, Indonesia) from GPS and earthquake slip vector data. *Journal of Geophysical Research: Solid Earth, 111*(B8)*,* B08409. https://doi.org/10.1029/2005JB003963

Spakman, W., & Hall, R. (2010). Surface deformation and slab-mantle interaction during Banda arc subduction rollback. *Nature Geoscience, 3*, 562-566. https://doi.org/10.1038/NGEO917

Stewart, G. S., & Cohn, S. N. (1979). The 1976 August 16, Mindanao, Philippine earthquake (M_s = 7.8) – evidence for a subduction zone south of Mindanao. *Geophysical Journal International, 57*(1), 51-65. https://doi.org/10.1111/j.1365-246X.1979.tb03771.x

Storchak, D. A., Harris, J., Brown, L., Lieser, K., Shumba, B., & Di Giacomo, D. (2020). Rebuild of the Bulletin of the International Seismological Centre (ISC) - part 2: 1980-

2010. *Geoscience Letters, 7,* 18. https://doi.org/10.1186/s40562-020-00164-6

Suhardja, S. K., Widiyantoro, S., Métaxian, J.-P., Rawlinson, N., Ramdhan, M., & Budi-Santoso, A. (2020). Crustal thickness beneath Mt. Merapi and Mt. Merbabu, central Java, Indonesia, inferred from receiver function analysis. *Physics of the Earth and Planetary Interiors, 302,* 106455. https://doi.org/10.1016/j.pepi.2020.106455

Supendi, P., Nugraha, A. D., Puspito, N. T., Widiyantoro, S., & Daryono, D. (2018). Identification of active faults in West Java, Indonesia, based on earthquake hypocenter determination, relocation, and focal mechanism analysis. *Geoscience Letters, 5*, 31. https://doi.org/10.1186/s40562-018-0130-y

Tate, G. W., McQuarrie, N., van Hinsbergen, D. J. J., Bakker, R. R., Harris, R., & Jiang, H. (2015). Australia going down under: Quantifying continental subduction during arc-continent accretion in Timor-Leste. *Geosphere, 11*(6), 1860-1883. https://doi.org/10.1130/GES01144.1

Tozer, B., Sandwell, D.T., Smith, W. H. F., Olson, C., Beale, J. R., & Wessel, P. (2019). Global bathymetry and topography at 15 arc sec: SRTM15+. *Earth and Space Science, 6*(10), 1847-1864. https://doi.org/10.1029/2019EA000658

Tregoning, P., & Gorbatov, A. (2004). Evidence for active subduction at the New Guinea trench. *Geophysical Research Letters*, *31*(13), L13608. https://doi.org/10.1029/2004GL020190

Tsutsumi, H., & Perez, J. S. (2013). Large-scale active fault map of the Philippine fault based on aerial photograph interpretation. *Active Fault Research, 2013*(39), 29-37. https://doi.org/10.11462/afr.2013.39_29

U.S. Geological Survey (2020). Advanced National Seismic System (ANSS) comprehensive earthquake catalog (ComCat). https://earthquake.usgs.gov/. Accessed 2020-07-28.

Valkaniotis, S., Ganas, A., Tsironi, V., & Barberopoulou, A. (2018). A preliminary report on the M7.5 Palu 2018 earthquake co-seismic ruptures and landslides using image correlation techniques on optical satellite data. https://doi.org/10.5281/zenodo.1467128

1459 Watkinson, I. M., & Hall, R. (2017). Fault systems of the eastern Indonesian triple junction:
1460 Evaluation of Quaternary activity and implications for seismic hazards. In P. R.
1461 Cummins, & I. Meilano (Eds.), *Geohazards in Indonesia: Earth Science for Disaster Risk*
1462 *Reduction,Geological Society, London, Special Publication,* (Vol. 441, pp. 71-120). The
1463 Geological Society of London. https://doi.org/10.1144/SP441.8

1464 Watkinson, I. M., Hall, R., & Ferdian, F. (2011). Tectonic re-interpretation of the Banggai-Sula-
1465 Molucca Sea margin, Indonesia. In R. Hall, M. A. Cottam, & M. E. J. Wilson (Eds.), *The*
1466 *SE Asian Gateway: History and Tectonics of the Australia-Asia Collision, Geological*
1467 *Society, London, Special Publications* (Vol. 355, pp. 203–224). The Geological Society
1468 of London. https://doi.org/10.1144/SP355.10

1469 Wessel, P., Luis, J. F., Uieda, L., Scharroo, R., Wobbe, F., Smith, W. H. F., & Tian, D. (2019).
1470 The Generic Mapping Tools version 6. *Geochemistry, Geophysics, Geosystems, 20*(11),
1471 5556-5564. https://doi.org/10.1029/2019GC008515

1472 Widiwijayanti, C., Tiberi, C., Deplus, C., Diament, M., Mikhailov, V., & Louat, R. (2004).
1473 Geodynamic evolution of the northern Molucca Sea area (eastern Indonesia) constrained
1474 by 3-D gravity field inversion. *Tectonophysics, 386*(3-4), 203-222.
1475 https://doi.org/10.1016/j.tecto.2004.05.003

1476 Widiyantoro, S., Gunawan, E., Muhari, A., Rawlinson, N., Mori, J., Hanifa, N.R., et al. (2020).
1477 Implications for megathrust earthquakes and tsunamis from seismic gaps south of Java
1478 Indonesia. *Nature: Scientific Reports, 10*, 15274. https://doi.org/10.1038/s41598-020-
1479 72142-z

1480 Widiyantoro, S., Pesicek, J. D., & Thurber, C. H. (2011a). Subducting slab structure below the
1481 eastern Sunda arc inferred from non-linear seismic tomographic imaging. In R. Hall, M.
1482 A. Cottam, & M. E. J. Wilson (Eds.), The SE Asian Gateway: History and Tectonics of
1483 the Australia-Asia Collision, *Geological society, London, Special Publications* (Vol. 355,
1484 pp. 139-155). The Geological Society of London. https://doi.org/10.1144/SP355.7

1485 Widiyantoro, S., Pesicek, J. D., & Thurber, C. H. (2011b). Complex structure of the lithospheric
1486 slab beneath the Banda arc, eastern Indonesia depicted by a seismic tomographic model.

Research in Geophysics, 1(1), e1. https://doi.org/10.4081/rg.2011.e1

Wiseman, K., Banerjee, P., Bürgmann, R., Sieh, K., Dreger, D. S., & Hermawan, I. (2012). Source model of the 2009 M_w 7.6 Padang intraslab earthquake and its effect on the Sunda megathrust. *Geophysical Journal International, 190*(3), 1710-1722. https://doi.org/10.1111/j.1365-246X.2012.05600.x

Wölbern, I., & Rümpker, G. (2016). Crustal thickness beneath Central and East Java (Indonesia) inferred from P receiver functions. *Journal of Asian Earth Sciences, 115*, 69-79. https://doi.org/10.1016/j.jseaes.2015.09.001

Wortel, M. J. R., & Spakman, W. (2000). Subduction and slab detachment in the Mediterranean-Carpathian region. *Science, 290*(5498), 1910-1917. https://doi.org/10.1126/science.290.5498.1910

Yang, X., Singh, S. C., & Tripathi, A. (2020). Did the Flores backarc thrust rupture offshore during the 2018 Lombok earthquake sequence in Indonesia? *Geophysical Journal International, 221*(2), 758-768. https://doi.org/10.1093/gji/ggaa018

Ye, L., Lay, T., & Kanamori, H. (2012). Intraplate and interplate faulting interactions during the August 31, 2012, Philippine trench earthquake (M_w 7.6) sequence. *Geophysical Research Letters, 39*(24), L24310. https://doi.org/10.1029/2012GL054164

Yeh, H., Imamura, F., Synolakis, C., Tsuji, Y., Liu, P., & Shi, S. (1993). The Flores Island tsunamis. *Eos*, *Transactions, American Geophysical Union, 74*(33), 369-373. https://doi.org/10.1029/93EO00381

Zhan, Z. (2020). Mechanisms and implications of deep earthquakes. *Annual Review of Earth and Planetary Sciences, 48,* 147-174. https://doi.org/10.1146/annurev-earth-053018-060314